Winter 2022

Reconstructing deglacial and Holocene climatic and environmental change in the Snowy Mountains of southeast Australia

Aidan Warner Burdick
Western Washington University, burdicka30@gmail.com

Reconstructing deglacial and Holocene climatic and environmental change in the Snowy Mountains of southeast Australia

By

Aidan Warner Burdick

Accepted in Partial Completion
of the Requirements for the Degree
Master of Science

ADVISORY COMMITTEE

Dr. Douglas H. Clark, Chair

Dr. Brady Z. Foreman

Dr. Allison M. Pfeiffer

GRADUATE SCHOOL

David L. Patrick, Dean

Master's Thesis

In presenting this thesis in partial fulfillment of the requirements for a master's degree at Western Washington University, I grant to Western Washington University the non-exclusive royalty-free right to archive, reproduce, distribute, and display the thesis in any and all forms, including electronic format, via any digital library mechanisms maintained by WWU.

I represent and warrant this is my original work, and does not infringe or violate any rights of others. I warrant that I have obtained written permissions from the owner of any third party copyrighted material included in these files.

I acknowledge that I retain ownership rights to the copyright of this work, including but not limited to the right to use all or part of this work in future works, such as articles or books.

Library users are granted permission for individual, research and non-commercial reproduction of this work for educational purposes only. Any further digital posting of this document requires specific permission from the author.

Any copying or publication of this thesis for commercial purposes, or for financial gain, is not allowed without my written permission.

Aidan Warner Burdick

March 2022

Reconstructing deglacial and Holocene climatic and environmental change in the Snowy Mountains of southeast Australia

A Thesis
Presented to
The Faculty of
Western Washington University

In Partial Fulfillment
Of the Requirements for the Degree
Master of Science

by
Aidan Burdick
March 2022

Abstract

Multi-proxy, long-term records of deglacial and Holocene climatic and environmental change in southeast Australia are rare, leaving the region a gap in local and large-scale synoptic climate reconstructions. The Snowy Mountains include the highest and coldest regions of mainland Australia and were the only part of the mainland that was glaciated during the late Pleistocene. Lakes formed by the glaciers have provided continuous sediment traps since glacial retreat following the Last Glacial Maximum. In this report, I reconstruct the maximum ice extents of glaciers during the last glacial period and estimate their equilibrium line altitudes, revising the work of Barrows *et al*. (2001) using recently published 2-m resolution lidar imagery. My remapping changes the extents of two out of the eleven identified glaciers and expands the total glaciated surface area to ~16 km^2, a 9% increase from that of Barrows *et al*. (2001).

I also construct an 18.2 kyr record of environmental change based on analyses of an 8.2 m sediment core from Blue Lake, the largest and deepest of the lakes in the Snowy Mountains. This record incorporates several proxies, including loss-on-ignition, magnetic susceptibility, laser grain size analysis, and several ratios derived from Xray fluorescence scans that serve as proxies for physical and chemical weathering in the catchment and as complementary measures of grain size and grain size variability. The Blue Lake record suggests that the environment was highly variable immediately following deglaciation. The Snowy Mountains experienced a cold and/or dry climate between 18.1 – 16.7 thousand calibrated years before present (cal ky BP) followed by warm and/or wet conditions between 16.7 – 16.3 cal ky BP, a return to cold and/or dry conditions from 16.3 – 15.8 cal ky BP, and a brief climate amelioration with relatively warm and/or wet conditions between 15.8 – 14.9 cal ky BP. A major shift between 14.9 – 12.6 cal ky BP reflects a largely devegetated landscape reflecting cool and/or dry climatic conditions that appears to coincide with the Antarctic Cold Reversal, a cold period identified in much of the

Southern Hemisphere south of 40 ºS. There is evidence for relatively warm and/or wet conditions during the period encompassing the Younger Dryas and earliest portions of the Holocene (12.6 – 10.8 cal ky BP). A clastic-rich interval dated to 10.8 – 9.7 cal ky BP suggests a final possible episode of cool and/or dry conditions in the early Holocene, but such an event has not been recognized elsewhere in Australia or the Southern Hemisphere. After ca. 9.7 cal ky BP, conditions appear to shift permanently to relatively stable, near-modern (relatively warm/wet) values overall, although there is evidence for possible cooling and/or drying coincident with the 8.2 ka event, as well as minor possible cooling/drying or increased fire impacts during an interval between 2.2 – 1.2 cal ky BP. Overall, the Blue Lake climate record bears more similarities to those of high Southern latitudes than to those in northern or tropical latitudes over the last 18.2 kyr, suggesting that southeast Australia's climate is synoptically tied to that of Antarctica, New Zealand, and Patagonia. Future work in the Snowy Mountains should focus on obtaining quantitative temperature and precipitation records throughout the whole deglacial and Holocene periods from all the glacial lakes to improve upon this record and identify catchment-specific effects.

Acknowledgements

While this project ultimately has my name on it, I owe gratitude to many people who have helped me complete this thesis. I am extremely grateful to everyone who contributed to the success of this project and who helped me grow as a scientist and as a person throughout the whole process. This project was completed mostly during the COVID-19 pandemic, which brought many unexpected challenges that required support from a great number of people. Thank you to my family: Mom, Dad, Lily, Claire, and Greta. I am deeply grateful to my wonderful partner Jenna – thank you for your unwavering love, support, understanding, and kindness in the hardest of times. Thank you to my friends at WWU: Callie, Ben, James, Delaney, Kalieh, Charles, Liam, and Julie. I appreciate all of you. I owe a massive thank you to Ben Paulson, without whom this project would have not been successful. Ben, thank you for your expertise, kindness, generosity, time, energy, and patience – I relied on you greatly throughout the project, and you always came through. I am so thankful for everything you have done for me and the whole department at WWU. I am also grateful for the scientists at other institutions who were essential in gathering much of the data for this project: Brady Shannon and Mark Shapley at LacCore, Robert Brown at the Large Lakes Observatory, and Susan Zimmerman at Lawrence Livermore National Laboratory. Thank you to my committee members, Allison Pfeiffer and Brady Foreman, for being generous with your time, energy, and insight. Finally, I offer a sincere thank you to my advisor, Doug Clark, who made this research possible despite the challenges brought by the pandemic. Thank you for your patience, generosity, support, and for giving me the opportunity to conduct this research.

I also would like to thank the funding sources who made this project possible: the NSF P2C2 EAGER program, the LacCore Visiting Graduate Student Program, the WWU Geology Department, and the WWU Graduate School.

Table of Contents

List of Tables and Figures

List of Tables:

List of Figures:

1. Introduction

The existing deglacial (~21–12 ka) and Holocene (12–0 ka) terrestrial climate record in southeast Australia is currently poorly constrained, inhibiting both regional and Southern Hemisphere reconstructions of climatic and environmental change. This is largely a result of Australia's aridity and dearth of perennial lakes, which limit the availability of high-quality continuous paleoclimate records. The result is that Australia is something of a "hole" in the existing post-Last Glacial Maximum (LGM, ~21 ka globally; Clark *et al.*, 2009) climate record of the Southern Hemisphere (e.g., Pedro *et al*., 2016). The Snowy Mountains of southeast Australia are the highest and coldest region of Australia and contain several perennial lakes that are well-suited for the development of paleoclimate records to help fill this gap. Perennial lakes often preserve excellent high-resolution proxy records of climatic and environmental change because they receive continuous sediment input that is closely linked to the climate system (Laird *et al.*, 1998). Variations in sedimentation patterns often reflect changes in atmospheric circulation and dust delivery (e.g., Harrison and Metcalfe, 1985; Stanley and De Deckker, 2002), changes in lake level corresponding to variations in temperature (e.g., Wilkins *et al.*, 2013), salinity and hydrological change corresponding to changes in precipitation and evapotranspiration (e.g., Woodward *et al.*, 2014), and shifts in vegetation dynamics within the catchment (e.g., Kershaw *et al.*, 2007).

Blue Lake is the largest of several alpine tarns located in Kosciuszko National Park (Figure 1), which encompasses the highest portions of the Snowy Mountains in southeastern Australia. The highest cirques in this area were periodically occupied by small glaciers during the last glacial cycle, including during the LGM (Barrows *et al*., 2001, 2002). Blue Lake, which formed immediately following retreat of the LGM glaciers, has existed continuously since that

time and therefore should contain a paleoenvironmental record with significance to southeast Australia and the Southern Hemisphere for several reasons. First, lakes at high elevation have been frequently documented as being particularly sensitive to even small changes in climate (e.g., Thompson *et al*., 2005; Woodward *et al*., 2014; Leunda *et al*., 2017). They also tend to preserve sediments in a relatively pristine state (e.g., Stanley and De Deckker, 2002; Bowerman and Clark, 2011). Second, Blue Lake is geographically well situated, as it lies in a region with few paleoclimate records, yet which is affected by several regional atmospheric transport pathways (e.g., Petherick *et al*., 2009). Finally, deglacial and Holocene climatic reconstructions from alpine regions in the Trans-Antarctic region (Antarctica, New Zealand, and Southern Chile), have shown synchronous and somewhat coherent climatic and environmental dynamics ("teleconnections") between locations (e.g., De Deckker *et al*., 2012; Pedro *et al*., 2016), but it is unclear if Australia also experienced these dynamics. Because of its geographical position and relatively high elevation, Blue Lake is among the best locations to test if these Southern Hemisphere climatic teleconnections are also present in southeast Australia. An additional benefit of studying Blue Lake is that analysis of the lake sediments in combination with the region's geomorphic features allows for reconstructions of glacial extents during the LGM and the local response to deglaciation. Although earlier studies (e.g., Barrows *et al*., 2001) have mapped the presumed extents of LGM glaciers in the region, recently collected lidar data (Gallant *et al.*, 2011) provide a new data set to further constrain the published mapping and to reconstruct maximum glacial extents. These higher resolution data justify re-mapping glacial extents, features, and deposits. These reconstructions in turn will provide valuable constraints on maximum temperature and precipitation conditions since deglaciation in the region.

In this study, I reconstruct the extent of glaciers in the Snowy Mountains during the LGM and present a record of climatic and environmental change from an 8.2 m sediment core collected from Blue Lake. The records presented here rely on several sensitive paleoclimate proxies, including sediment grain size, geochemical paleoclimate proxies derived from Xray fluorescence (XRF), magnetic susceptibility, and loss-on-ignition (LOI; an indicator of sediment organic content). I analyze these proxies in combination to assess the nature and magnitude of climatic and environmental change at Blue Lake over the last ca.18 ka and to determine whether sediments at Blue Lake record major hemispheric climate fluctuations (e.g., Antarctic Cold Reversal, Younger Dryas, the 8.2 ka event, Little Ice Age) and, if present, to assess their magnitudes and characteristics in the Snowy Mountains.

The paleoclimate reconstruction from Blue Lake should have several valuable outcomes. The analyses should provide important context for paleoclimate models in Australia and the Southern Hemisphere and thereby assist with environmental planning for local communities, agencies, and utilities (e.g., Australian National Parks; Snowy Hydro, a local power and water utility). The record will also inform how the region has responded to climate shifts in the past, which is essential to prepare for modern climate change. This study is planned to be the first in a series of studies that will involve analyses of cores from other lakes in the high Snowy Mountains which will incorporate several other paleoclimate proxies (e.g., biomarkers, isotopic geochemistry, etc.) that were not feasible in my study because of travel restrictions related to the COVID-19 pandemic. By establishing a rigorous model of climatic and environmental change at Blue Lake, this study will provide a sedimentologic foundation for those further studies that will reconstruct other environmental parameters such as drought and wildfire frequency. Understanding how these phenomena have evolved through time is essential for Australia, which

has experienced extreme drought and wildfire in the last few years. Finally, better constraints on climate in mountainous regions is critical to understanding regional erosion and sediment transport dynamics (Allen, 2008), and therefore these records can strengthen the existing understanding of Earth surface processes in southeastern Australia on human and millennial timescales.

2. Background

2.1 Regional setting

The study site is located in Kosciuszko National Park (KNP) in New South Wales about 140 km SSW of Canberra (Figure 1). KNP contains the highest portions of the Snowy Mountains, including Mt. Kosciuszko, mainland Australia's tallest mountain (2,228 m above sea level; Figure 1). The Snowy Mountains are part of the Lachlan Geosyncline of eastern Australia, with bedrock primarily consisting of large swaths of Paleozoic igneous and sedimentary rocks (Kolbe and Taylor, 1966). The igneous rocks in KNP comprise late Ordovician basalts and metabasic intrusives as well as late Silurian to early Devonian leucogranite and granodiorite with metasedimentary xenoliths. The sedimentary rocks are late Ordovician in age and consists of interbedded shales, siltstones, and fine-grained sandstones forming deep marine turbidite sequences (Kolbe and Taylor, 1966; Wyborn *et al.*, 1990). The exact timing of the Kosciuszko Block's uplift is contested, but certainly occurred at least partly during the early Miocene and may have lasted from the Eocene through the Pliocene (Sharp, 2004).

2.2 Blue Lake

Blue Lake (36°24’11”S, 148°18’57”E) is a small dimictic tarn in KNP formed during the most recent glacial cycle (Figure 2). The lake is situated at an elevation of 1890 m and has a surface area of 0.14 km^2 and a catchment area of 2.2 km^2. The lake has two primary depo-basins, one near the center of the lake and one closer to the lake’s outlet (Blue Lake Creek), both with maximum depths of ca. 28 m (Raine, 1982; Figure 2). There are two sources of instrumental climate data near Blue Lake at similar elevations: the Thredbo weather station (36º29’24”S, 148º17’24”E, elevation 1,957 m; Figure 1) and the Charlotte Pass weather station (36º25’40”S, 148º20’1”E, elevation 1,730 m). The Thredbo station has a mean summer maximum temperature of 15.7 °C, a mean winter maximum temperature of 0.7 °C, and a mean annual rainfall of 1410 mm/yr (measured from 1966-2021; extracted from the Australian Bureau of Meteorology at bom.gov.au). The Charlotte Pass weather station has a mean summer (Dec.-Feb.) maximum temperature of 16.9 °C, a mean maximum winter (June, July, Aug.) temperature of 2.6 °C, and a mean annual rainfall of 1950 mm/yr (measured from 1930-2015; extracted from the Australian Bureau of Meteorology at bom.gov.au). Average wind speed at both stations is highly variable throughout the year, but peaks in the Austral winter, averaging about 30 km/hr.

The surface of Blue Lake freezes over completely in most winters, although it has frozen partially during exceptionally mild winters (Burgess *et al.*, 1988). The modern lake water typically has low turbidity values and a neutral pH (Balmaks, 1984; Stanley and De Deckker, 2002). Bedrock in the Blue Lake catchment is dominated by broad NNE-SSW striking bands of sedimentary rocks and two granitic plutons that crop out throughout the basin; the bedrock is covered locally by variable thicknesses of regolith and till, along with small areas of thin peaty sediments (Figure 4**;** Wyborn *et al*., 1990; Stanley and De Deckker, 2002).

2.2.1 Climate sensitivity at Blue Lake

Alpine lakes with small catchments are considered to be particularly sensitive to climatic and environmental changes (e.g., Thompson *et al*., 2005; Leunda *et al*., 2017). In such catchments, air temperature commonly controls both snow cover and primary productivity in the lake, and thus small fluctuations can result in large magnitude changes in lake sediment deposition (e.g., Thompson *et al*., 2005; Woodward *et al*., 2014; Leunda *et al*., 2017). Moreover, lakes with small catchments without large groundwater inputs are especially sensitive to variations in precipitation (e.g., Cardille *et al*., 2004). Therefore, Blue Lake is an ideal site to investigate post-LGM climatic and environmental changes in southeastern Australia.

2.3 Modern climate and climate drivers of southeast Australia

2.3.1 Modern climate of southeast Australia

The modern climate of southeast Australia is similar to the Mediterranean region with hot dry summers and cool wet winters (Gouramanis *et al.*, 2013). Mean annual sea-surface temperatures in the Tasman Sea to the east and southeast of KNP vary between 16 and 20 ºC (Barrows and Juggins, 2005). The primary source of winter precipitation in the Snowy Mountains is the mid-latitude westerlies, which shift southward during the summer because of changes in insolation in the Inter-Tropical Convergence Zone (ITCZ; Gouramanis *et al.*, 2013). Several climate variables affect southeastern Australia, including the Southern Hemisphere westerly winds, the Southern Annular Mode, the El Niño-Southern Oscillation, and the Indian Ocean Dipole, which are discussed in greater detail below.

2.3.2 Southern Hemisphere westerlies

The southern westerlies are a primary source of moisture to southeastern Australia (Gouramanis *et al*., 2013), they affect regional dust transport and aeolian sedimentation (e.g., Petherick *et al*., 2009), influence concentrations of atmospheric CO_2 (Toggweiler *et al*., 2006), and modulate and respond to the other atmospheric and oceanic phenomena discussed in this section (e.g., McGee *et al.*, 2018; Jiang and Yan, 2020). The major atmospheric jets comprising the southern westerly winds are the subtropical westerly jet, which is centered on 30°S and is driven by subtropical Hadley Cell transport, and the subpolar westerly jet, which is centered around 50°S and is driven predominantly by eddies created by the subtropical westerly jet (Lee and Kim, 2003; Jiang and Yan, 2020). Several factors affect the positions and strengths of these westerly jets including orbital insolation, greenhouse gas concentrations, and Antarctic ice sheet topography (Jiang and Yan, 2020).

2.3.3 Southern Annular Mode

The Southern Annular Mode (SAM), also referred to as the Antarctic Oscillation, is defined as the difference in zonal mean sea level air pressure between 40°S and 65°S (Gong and Wang, 1999). The positive phase of the SAM is associated with higher sea level pressure at 40°S than 65°S, resulting in a southward shift in the westerly winds, whereas the negative phase is associated with higher sea level pressure at 65°S than 40°S and a northward shift in the westerly winds (Gong and Wang, 1999; Gouramanis *et al*, 2013). In southeast Australia, the positive phase of the SAM is associated with decreased precipitation during the autumn and winter and increased precipitation during the spring and summer, and vice-versa for the negative phase (Hendon *et al*., 2007; Gouramanis *et al*., 2013).

2.3.4 El Niño-Southern Oscillation

The El Niño-Southern Oscillation (ENSO) is a recurring annual to decadal-scale variation in sea surface temperatures and atmospheric pressure in the eastern Pacific that has an important effect on global climate, including in Australia. Variations in atmospheric pressure across the Pacific alter sea surface temperatures, which in turn cause changes in oceanic circulation. These system-wide changes result in shifts in global climate, which are subdivided into the El Niño phase, the La Niña phase, and the neutral phase. The El Niño phase occurs when sea surface temperature anomalies in the Niño 3.4 region (5°N–5°S, 120°–170°W) exceed 0.4 °C or more (Trenberth, 1997). In southeastern Australia, this typically results in warmer and drier than average conditions (Australian Bureau of Meteorology, 2014). In contrast, the La Niña phase is the cool phase of ENSO, where sea surface temperature anomalies are low; typically, the La Niña phase is associated with cooler and wetter conditions in southeastern Australia (Australia Bureau of Meteorology, 2016). The neutral phase is generally associated with average temperature and precipitation conditions across regions affected by ENSO (NOAA Climate Prediction Center, 2012).

2.3.5 Indian Ocean Dipole

The Indian Ocean Dipole (IOD) is the difference in sea surface temperatures between the equatorial western Indian Ocean (10°S to 10°N, 50°E to 70°E) and the eastern Indian Ocean (10°S to 0°S, 90°E to 110°E; Saji *et al*., 1990; Gouramanis *et al*., 2013). The positive mode is generally associated with decreased winter and spring precipitation in much of Australia, whereas the negative mode is generally associated with increased winter and spring precipitation

(Australian Bureau of Meteorology, 2013). A synthesis of modern on climate drivers found that the effects of the IOD are small in southeast Australia, but that in some instances it can influence precipitation (Gouramanis *et al*., 2013).

2.4 The bipolar seesaw and Trans-Australian teleconnections

During the most recent deglaciation, the Northern and Southern Hemispheres experienced synchronous but inverse millennial-scale climate anomalies in a phenomenon known as the "bipolar seesaw" (e.g., De Deckker *et al*., 2012; Pedro *et al*., 2016). During these millennial-scale anomalies, one hemisphere typically experienced warmer and wetter conditions while the other experienced cooler and drier conditions. In the Southern Hemisphere, the climates of Antarctica, New Zealand, the southern portions of South America (e.g., the Southern Andes and Patagonia), and Tasmania (hereafter referred to as the Trans-Australian region) have been linked (e.g., Pedro *et al*., 2016) due to similar climatic conditions during the deglacial and Holocene. Due to a lack of proxy data, however, it is not clear if the climate of southeastern Australia is consistent with the rest of the Trans-Australian region (e.g., Pedro *et al*., 2016); a focus of this study is to assess the degree to which the climatic and environmental conditions observed in the Snowy Mountains relate to other records from the region.

2.5 Glacial History of the Snowy Mountains

In this section I review the current understanding of glaciations in the Snowy Mountains spanning the latest Pleistocene and the LGM.

2.5.1 Late Pleistocene glaciations

Evidence of Pleistocene glaciation in KNP, although subtle compared to many glaciated mountains, is present (Figure 5), including moraine sequences at Blue Lake, Lake Cootapatamba, and to the northeast of Blue Lake as well as glacial flutes near Blue Lake, in several cirques, and the presence of five tarns in overdeepened basins (e.g., Barrows *et al*., 2001; Colhoun and Barrows, 2011). There is evidence for at least two distinct glaciations in KNP during the Late Pleistocene. ^{10}Be exposure dates of a moraine sequence at Blue Lake (Figure 5) indicate an Early Kosciuszko glaciation during Marine Isotope Stage (MIS) 4 with a single moraine dated between 57.7 ± 3.8 ka and 52.9 ± 2.7 ka (Snowy River Advance, Colhoun and Barrows, 2011; Barrows *et al.*, 2001; Doughty *et al*., 2021). No analogous glacial advance has been documented in Tasmania (Barrows *et al.*, 2002) during this interval. The moraine used to date the Early Kosciuszko glaciation, however, includes two younger exposure ages (43.5 ± 2.4 ka and 40.3 ± 2.1 ka) that fall into MIS 3 (Barrows *et al*., 2001; Doughty *et al*., 2021), and which may correspond to an advance observed on the North Island of New Zealand (Shulmeister *et al.*, 2019). Additionally, exposure dates from moraines at three sites in Tasmania (Lake Hartz, Lake Nichols, and Mt. Jukes) suggest advances occurred there between 46 and 39 ka, which closely align with these two dates (Barrows *et al*., 2002).

A subsequent glacial period, termed the Late Kosciuszko glaciation (LKG), occurred during MIS stages 2 and 3 and produced moraines dated to 32.0 ± 2.5 ka (Headley Tarn Advance), 19.1 ± 1.6 ka (Blue Lake Advance), and 16.8 ± 1.4 ka (Mt. Twynam Advance; Barrows *et al.*, 2001), which are broadly centered on the global LGM (26.5–19 ka; Clark *et al.*, 2009). Since the publication of these dates by Barrows *et al.* in 2001, however, there have been changes in standard sampling protocols, analytic methods, and calibration for CRN exposure

dating, and although the MIS 4 dates have been recalculated by Doughty *et al*. (2021), the ages from MIS 2 and 3 have yet to be recalculated.

2.5.2 The Last Glacial Maximum (22 – 18 ka)

In Australia, the LGM period lasted from ca. 22 ka to 18 ka (Reeves *et al.*, 2013), although Petherick *et al*. (2017) have argued for expanding the LGM to 33 to 18 ka based on a regional low in solar insolation and high levels of aeolian sedimentation in eastern Australia. The Snowy Mountains were the only demonstrably glaciated region in mainland Australia during the LGM. The timing of the LGM in KNP appears to be consistent with other glaciated regions in the trans-Australian region. The Blue Lake Advance (19.1 ± 1.6 ka, Barrows *et al.*, 2001) corresponds to the latter end of the global LGM (Clark *et al.*, 2009). This is also roughly consistent with the timing of the LGM elsewhere in the Southern Hemisphere, as reflected in Tasmania, where maximum ice extents persisted until between 17.3 ± 1.1 ka (^{10}Be ages from moraines) and 20.1 ± 1.9 ka (^{36}Cl ages; Barrows *et al.*, 2002), New Zealand (between 21 and 17 ka; Shulmeister *et al*., 2019), Papua New Guinea (19.4 ka; Barrows *et al.*, 2011), and the Southern Andes (c. 23 to 14 ka; Kaplan *et al*., 2004; Douglass *et al*., 2006).

Regional syntheses of Australian climate suggest a high degree of spatial variability in temperature and precipitation during the LGM. Based on his mapped glacier extents at KNP, Galloway (1965) estimated that mean temperatures in the summer months at the peak of the LGM were 9 ºC cooler than modern in KNP. This likely overestimates actual conditions because his mapped ice extents are substantially larger than that of Barrows *et al*. (2001) or as documented in my mapping. Other locations in the trans-Australia region show high variability in reconstructed cooling during the LGM. Chang *et al.* (2015) estimate that mid-summer

temperatures were about 6.5 ºC cooler than modern during the LGM at North Stradbroke Island (Figure 6). In the Tasman Sea southeast of KNP the LGM sea surface temperature anomaly from modern varies between 1 and 5 ºC cooler (Barrows and Juggins, 2005), although reconstructions from the southern portions of the Tasman Sea suggest that this cooling may have been as much as 5 to 7 ºC (Petherick *et al.,* 2013). Paleotemperature estimates from Papua New Guinea suggest LGM cooling there may have been as great as 11º C (Hope, 2009).

Uncertainty also persists about LGM precipitation patterns at KNP and across southeastern Australia. Raine (1974) produced a paleo-precipitation record at Blue Lake based on pollen analyses, but because the core did not reach the lake's basal sediments, there is no evidence for precipitation patterns prior to ca. 17 ka. Large uncertainties in the age-model for this core also limit its temporal resolution. A prominent hypothesis from other locations in southeastern Australia is that the LGM was relatively arid, which is supported by a decrease in rainforest taxa in pollen records from Lake Euramoo in northeastern Queensland (Haberle, 2005). These arid vegetation assemblages overlap with minima in precipitation levels at North Stradbroke Island from 24.5 to 20 ka (Petherick *et al.*, 2017). Conversely pollen assemblages from Little Llangothlin Lagoon in New South Wales indicate a relatively moist climate at the end of the LGM (Ellerton *et al.,* 2017), suggesting there was regional variability.

2.6 Deglacial and Holocene climate

Records of climatic and environmental change spanning the entire deglacial period and Holocene in southeast Australia are exceedingly rare. While most records span only a portion of this period, the current state of knowledge across this entire period can be illustrated with a

synthesis of published records. In this section, I highlight some of the key periods and climate events that are of interest in this study.

2.6.1 Deglacial period and Antarctic Cold Reversal (~18 – 12 ka)

The deglacial period (~18 – 15 ka) is a period characterized by a rapidly changing climate across the globe. As the Northern Hemisphere's ice sheets retreated and disappeared, temperatures rose rapidly and fundamentally altered most of Earth's environments, but in many cases climate cooled and warmed in stages on short timescales, including in Australia (e.g., Reeves *et al*., 2013). Records of deglacial climate are rare in Australia and constraining the nature and timing of climatic change during this period can help refine our understanding of abrupt climate change through this interval.

Immediately following the early deglacial period, the Antarctic Cold Reversal (ACR, 14.7 – 13.0 ka) was a major climate anomaly in the Southern Hemisphere roughly coincident with the Bølling–Allerød warm stage in the North Atlantic (Pedro *et al*., 2016). The ACR brought cool temperatures across much of the mid-and high southern latitudes, particularly in the south Atlantic and south of 40 ºS leading to glacial advances in Antarctica, the Andes, and New Zealand (e.g., Putnam *et al*., 2010; Pedro *et al.*, 2016; Mendelová *et al.*, 2020). The degree to which southeastern Australia experienced climate change brought by the ACR remains largely unconstrained (e.g., Pedro *et al*., 2016), and thus a goal of this study is to determine if the Snowy Mountains were affected.

Finally, The Younger Dryas (12.9 – 11.7 ka; Rasmussen *et al*., 2006) was a period of intense cooling and a return to nearly full-glacial conditions that affected much of the Northern Hemisphere, but its presence and impact in the Southern Hemisphere has been a source of

controversy (e.g., Reasoner *et al*., 1994; Goede *et al*., 1996; Andres *et al*., 2003; Barrows *et al*., 2007; García-Ruiz *et al*., 2012; Glasser *et al*., 2012; Hinojosa *et al*., 2019). Presently, the number of studies addressing the Younger Dryas in southeast Australia is small and determining the nature of environmental and climatic change in the Snowy Mountains during the Younger Dryas is a goal of this project.

2.6.2 Holocene and major Holocene climate events

The Holocene (12 – 0 ka) is the most recent geological epoch encompassing Earth's history following the most recent glacial period. Throughout much of the world, including Australia, the Holocene is characterized by warmer and wetter conditions than occurred during the glacial and early deglacial periods. In southeast Australia, climate appears to have been warm, wet, and relatively stable, but existing records indicate spatial and temporal variability (e.g., Fitzsimmons *et al*., 2013), and investigating this variability can enhance our understanding of past and future climate change.

There are two Holocene climate events that I assess in detail throughout this report. First, the 8.2 ka event is one of the most dramatic instances of abrupt climate change that occurred during the early Holocene. In the North Atlantic region, and particularly in Greenland, where the event was first identified, temperatures dropped by up to 3.3 ± 1.1 ºC and snow accumulation decreased in less than 20 years (Kobashi *et* al., 2007; Thomas *et al*., 2007). Overall, the cold event lasted about 150 years before climate amelioration occurred (Kobashi *et al*., 2007). The 8.2 ka event is well established in much of the Northern Hemisphere, but it is unclear to what extent it affected portions of the Southern Hemisphere.

Finally, the Little Ice Age was a period of minor cooling (less than 1 ºC globally), particularly evident in the Northern Hemisphere but which triggered glacial advances globally generally between the 15th to 19th centuries. Heterogeneities in the timing of these advances (and in associated non-glacial changes) indicate, however, that events linked to the Little Ice Age were not synchronous globally (Mann, 2002; Mann *et al*., 2009). The degree to which the Little Ice Age (and more broadly, neoglaciation) affected Australia remains unclear, in large part due to a dearth of proxy data from that period (e.g., Mann *et al*., 2009).

3.0 Methods

3.1. Glacial mapping

Barrows *et al*. (2001) produced a map of maximum ice extents at KNP during the LGM using observations from a 25-m digital elevation model and field mapping of glacier and snow landforms. Since this publication, new 2-m lidar data of KNP have been published (Gallant *et al*., 2011), allowing for higher-resolution digital mapping. I used the new lidar data in conjunction with high-resolution Google Earth imagery to revise the maps of glacial features and extents from Barrows *et al*. (2001). I defined maximum ice limits using glacial features and landforms including the outermost moraines, arcuate cirque headwalls, flutes, trim lines, hummocky deposits, and where possible, stream channel morphology.

3.2. Glacial equilibrium line altitude estimates

Based on my mapping of maximum ice extents at KNP, I used two methods, accumulation-area ratio (AAR) and area-altitude balance ratio (AABR) to estimate the equilibrium line altitudes (ELA) of the maximum positions of the former glaciers (e.g.,

Osmaston, 2005; Pellitero *et al*., 2015). Reconstructed ELAs provide a means to estimate baseline paleoclimate conditions at the LGM, immediately preceding onset of sedimentation in Blue Lake. The AAR is the ratio between the areas of the accumulation and ablation zones of a glacier (Osmaston, 2005; Pellitero *et al*., 2015). For estimates using the AAR method, I used an AAR of 0.60 based on modern glaciers with similar altitude and climate characteristics (Rea, 2009). I determined the ELA by drawing a reasonable equilibrium line across an interpolated glacier surface at a consistent elevation that satisfied the condition that 60% of the glacier surface was in the accumulation zone.

AABR uses an assumed accumulation area ratio similar to the AAR method, but also considers the mass-balance gradient and hypsometry of a glacier (Pellitero *et al*., 2015). However, AABR requires a known balance ratio for a given area; in regions that are not presently glaciated (such as KNP), the balance ratio cannot be determined directly and so one must be assumed (Rea, 2009; Pellitero *et al*., 2015). For this study, I use a well-established balance ratio of 3.333 based on empirical studies of modern Cascade glaciers (Rea, 2009) as there are presently no available balance ratio data or estimates from the Snowy Mountains. I calculated ELAs on my mapped Snowy Mountain glaciers using the ELA toolbox in ArcGIS (Pellitero *et al*., 2015).

3.3 Catchment analysis

I conducted a geospatial analysis of the Blue Lake catchment to determine the source areas of terrestrial organic matter and clastic sediment deposited in Blue Lake. The catchment draining Blue Lake was calculated using the Watershed tool in ArcGIS Pro and the digital elevation model and Lidar data from Gallant *et al*. (2011). Additionally, to assess the relative

sediment contribution of the catchment's tributaries, smaller "sub-watersheds" were determined from Blue Lake's three major tributaries – one feeding the northern edge of the lake, and two streams feeding the western edge of the lake. Pour points were selected as close to stream outlets into Blue Lake as possible with the caveat that the closest points sometimes yielded unreasonable calculations based on the processed flow accumulation rasters. Therefore, in some instances, pour points were moved slightly upstream.

3.4 Core acquisition

An 8.2-m sediment core (core ABL16-LI) was collected from Blue Lake on July 14, 2016 using a standard Livingstone piston corer from the frozen lake surface. The Livingston coring system comprises a 50.8 mm x 1 m core barrel, connected to the lake surface by 1.5-2 m mag-zirc extension rods (Livingstone, 1955; Wright, 1980). Successive 1 m cores were collected by pushing the core barrel into the mud while maintaining suction with an internal piston cabled to the surface; once a barrel is filled, the entire column is lifted out of the water, the core barrel is disconnected, then a new barrel is attached, and the process is continued. In order to reenter the hole at the bottom of the lake with each successive push, 4" PVC drainage pipe was used as casing from the frozen lake surface to the lake bottom. The cores were extruded in the field into 50.8 mm PVC tubes, double wrapped with commercial plastic wrap, and transported to ANSTO (https://www.ansto.gov.au/) for storage and initial analysis.

3.5 Sediment classification

3.5.1 Preliminary imaging and scans

At ANSTO, core segments were split into archive and working halves and stored in a refrigerated room until they were transported to the United States in October 2020 for analyses at the National Lacustrine Core Facility (LacCore) and Western Washington University. The cores were also scanned on the ITRAX XRF scanner at ANSTO, but unfortunately detailed results were inadvertently lost because of local personnel changes. A suite of macrofossil and bulk organic sediments were also collected for dating purposes, but those samples were unfortunately lost in transit to Western Washington University. The archive halves were shipped to LacCore for imaging and non-invasive scans. The sediment surface was cleaned using rounded glass microscope slides. The core segments were then imaged and logged on the GeoTek XYZ core scanner, which recorded point-sensor magnetic susceptibility, color spectra from 360 to 740 nm wavelengths in 10 nm steps, and L*a*b color values at 0.5 cm resolution. Visual descriptions were performed on the core images in the programs Corelyzer v. 2.1.1 and PSICAT v. 1.0.1 with references from smear slides taken throughout the core.

3.5.2 Unit and lithofacies designations

After initial core scans, I characterized the sediments and established primary sedimentary units. I considered several sediment characteristics such as color, grain size, clast size, the presence of sedimentary structures (e.g., laminae, turbidites), the nature of contacts between intervals, and any deformation or disturbances from coring or core transport. I also used smear slides to determine the presence of diatoms and search for other minor modifiers such as the remains of plants and aquatic organisms. I also paid particular attention to the nature of

contacts between units, noting if they were abrupt or diffuse. After classifying units, I developed a lithofacies model that characterizes the likely depositional conditions for similar units.

3.6 Grain size analysis

Grain size analyses are commonly performed in paleolimnological studies to determine the composition of clastic sediments and make inferences about their origin and processes of transportation. A variety of grain size parameters can be assessed through laser diffraction, including the fractions of clay (< 3.91 µm), silt (3.91 – 62.5 µm), and sand (62.5 µm – 2 mm), the 10th percentile (D_{10}), 50th percentile (D_{50}), and 90th percentile (D_{90}) of the grain sizes in a sample, and SPAN, a dimensionless parameter used to determine the degree of sorting (Equation 1; Foster *et al*., 1991).

$$SPAN = \frac{D_{90} - D_{10}}{D_{50}} \qquad \text{(Eqn. 1)}$$

In general, grain size is a primary indicator of the energy level of a lake environment and its catchment (Last, 2001). The interpretation of fluctuations in grain size depends on several factors such as lake depth, bathymetry, sediment source, slope stability, the strength of streamflow in and out of the lake, the presence of within-lake currents, and fire (Campbell, 1997). Because Blue Lake is relatively deep and small, contains steep sides that are potentially subject to slumping, and has small inlet and outlet streams, sediments deposited even deep in the lake should at least partially reflect changes in stream discharge and creek bedload conditions. Ohlendorf *et al*. (2003) demonstrated that coarse particles in alpine lake sediments likely indicate greater hillslope erosion whereas shifts towards finer particle distributions may reflect greater influence of fluvial transport, higher amounts of vegetation in the catchment, and a switch from primarily physical to chemical weathering.

To analyze the grain size composition of the core, the working halves of core ABL16-LI were sampled at 2 cm resolution and at 1 cm intervals in select intervals in the lower half of the core where grain size fluctuations were of particular interest, and often more closely spaced. Samples were treated with hydrogen peroxide (H_2O_2) to remove organic matter and with sodium hydroxide (NaOH) to remove diatoms according to LacCore Standard Operating Procedures http://lrc.geo.umn.edu/laccore/procedures.html). The NaOH reaction was neutralized with hydrochloric acid (HCl) to prevent the dissolution of clastic particles and rinsed with deionized water. Grain size was then measured using laser diffraction on a Malvern Mastersizer 2000 with HydroG cell and autosampler. Each aliquot was measured three times to ensure replicability.

3.7 Loss-on-ignition

Loss-on-ignition (LOI) is a common procedure used to estimate the concentration of organic matter in sediments. LOI is common because it is relatively inexpensive, accurate, and users can efficiently run large numbers of samples. In lake sediments, the mass of sediment lost during combustion at 550 °C has been shown to closely correlate to carbon content determined through chromatography (Dean, 1974). Moreover, when the procedure is performed using a consistent operating procedure, LOI can be a useful tool for making relative comparisons with other sediment cores (Heiri *et al*., 2001). In conjunction with elemental ratios determined with Xray fluorescence, LOI should be a reliable relative indicator of the abundance of organic content in core ABL16-LI.

Organic matter found in lake sediments is typically derived from aquatic and terrestrial plant detritus, although small concentrations (usually < 10%) can be derived from animals (Meyers and Ishiwatari, 1995). The concentration of organic matter can be indicative of lake

productivity and vegetation cover in the catchment, which frequently respond to regional changes in temperature and precipitation. In non-glacier-fed lakes, lake productivity has been linked to surface summer air temperature (Nesje and Dahl, 2001), with the general relationship being that higher productivity (higher LOI) is associated with warmer summer air temperatures. Moreover, wetter climates are associated with increased deposition from plant detritus sourced from the catchment (Meyers and Lallier-Vergès, 1999). Low LOI has also been linked to low vegetation cover and higher rates of physical weathering and erosion within a catchment (Beer *et al*., 2007). Higher LOI should therefore be an indicator of overall warmer and wetter conditions at Blue Lake, and insight from other proxies will assist in determining the relative importance of temperature and precipitation in observed changes in the Blue Lake sedimentary sequence.

LOI concentrations were determined following LacCore standard operating procedures (http://lrc.geo.umn.edu/laccore/assets/pdf/sops/loi.pdf). The working halves of core ABL16-LI were sampled at 2 cm resolution where possible (~1 cm^3 samples), although in select intervals, samples were spread apart further due to sediment underfilling and water loss during storage. For each measurement, the empty sample crucible was weighed with precision to 0.1 mg, and then weighed again after adding the sediment sample. The crucibles were then placed in a drying oven for at least 12 hours at 100°C to remove water. The samples were allowed to cool in a desiccation chamber and weighed again. The samples were then placed in a furnace at 550°C for 4 hours to remove organic content, allowed to cool, and weighed a final time. LOI was then calculated using Equation 2:

$$LOI\ (\%) = \left(\frac{Wt_{dry} - Wt_{ignition}}{Wt_{dry}}\right) * 100 \qquad \text{(Eqn. 2)}$$

3.8 Xray fluorescence scans

The concentrations and ratios of elements determined through Xray fluorescence (XRF) scans are frequently used to reconstruct a variety of climatic and environmental variables (e.g., Davies *et al*., 2015). In this study, I use XRF data to assess weathering in the Blue Lake catchment and to provide a secondary proxy for grain size.

The rate of weathering in a lake catchment is often related to shifts in temperature and precipitation, although other controls on weathering such as soil thickness and vegetation cover are important considerations (West *et al*., 2005). Periods with cooler temperatures and lower precipitation result in lower rates of chemical weathering compared to physical weathering (e.g., Brady and Carroll, 1994). The primary XRF proxy for catchment weathering is the rubidium/strontium (Rb/Sr) ratio, where lower Rb/Sr ratios in lake sediments are associated with higher rates of chemical weathering in the catchment (e.g., Jin *et al*., 2006). Because of the relationship between climate and weathering, the Rb/Sr ratio (often reported as log(Rb/Sr)) has been used to reconstruct the precipitation-to-evaporation (P/E) ratio and relative temperature changes (e.g., Heymann *et al*., 2013; Fernández *et al*., 2013). Additionally, the K/Ti ratio has been used to assess the degree of weathering in alpine lake catchments. Decreased K/Ti ratio values in these sediments have been interpreted as indicating an increase in chemical weathering (e.g., Arnaud *et al*., 2012; Davies *et al*., 2015; Bastian *et al*., 2017).

Several elemental concentrations are associated with minerogenic inputs into lakes, and their concentrations can be used as indicators of changes in grain size. K, Ti, and Rb are associated with clay minerals, whereas Zr and Si are associated with silt- and sand-sized fractions (Kylander *et al*., 2011, 2013). In this study, I use XRF scans to assess grain size variability; XRF scans have a much finer resolution than the laser particle-size analyses. I use

three XRF ratios for grain size. First, I use Si/Ti, which should positively correlate with the concentration of sand (e.g., Moreno *et al*., 2007). I also use K/Zr (e.g., Cuven *et al*., 2011), which should positively correlate with finer grain size. Finally, I use Zr/Rb (e.g., Kylander *et al*., 2011), which should positively correlate with a coarser overall grain size composition.

Xray fluorescence (XRF) scans were conducted on the ITRAX XRF Corescanner at the Large Lakes Observatory (LLO) at the University of Minnesota Duluth. The cores were scanned in a Cr source tube at 30 kV and 55 mA with a 1 mm resolution and 15 s dwell time. The data were normalized to coherent scattering to account for variable water content in the cores and condensed with a 1 cm moving average. Data were removed from intervals where the sediment surface was too low, or the instrument reported an invalid measurement. X-radiographic images were taken at 60 kV and 30 mA with a 0.2 mm step size for between 150 and 400 ms depending upon the section.

3.9 Chronology

I developed an age model for core ABL16-LI using ^{14}C Accelerator Mass Spectrometry (AMS) dating of macrofossils wherever possible; lack of macrofossils in some crucial intervals in the bottom sections of the core, however, required dating of bulk sediments. Radiocarbon dating was conducted at the Center for Accelerator Mass Spectrometry at Lawrence Livermore National Laboratory (LLNL). Radiocarbon ages were calibrated using CALIB (version 8.2; Stuiver *et al*., 2021) and the SHCal20 curve (Hogg *et al*., 2020). I used three plant macrofossil and four bulk organic samples; two of these bulk sediment samples were paired with macrofossils to establish a reservoir effect but were not included in the age-depth model. To develop an age-depth model, I used the R program Bacon (Bayesian accumulation), which uses

radiocarbon dates to reconstruct accumulation histories in sedimentary deposits while incorporating uncertainties (Blaauw and Christen, 2011).

4. Results

4.1 Glacial mapping and LGM equilibrium line altitude estimates

My remapping of the LGM glacial extents in the Snowy Mountains indicates a total glaciated surface area of approximately 16.4 km^2, which is about 9% greater than that indicated by Barrows *et al*. (2001, Figure 7). Many of my estimates of maximum ice extents are similar to Barrows *et al*. (2001), but there are notable differences in several cirques. I also made adjustments to the extents of two glaciers in comparison to Barrows *et al*. (2001); this involved a reduction of glacier KM_8 and an increase in glacier KM_5 (Figure 7). Estimates of ELAs for LGM glacial extents in the Snowy Mountains using the AAR method vary from 1,810 to 2,065 meters with an average ELA of about 1,968 meters and a standard deviation of about 65 meters (Table 1, Table 2, Figure 8). ELA estimates for maximum glacial extent using the AABR method vary from 1,825 to 2,085 meters with an average ELA of about 1,965 meters and a standard deviation of about 65 meters (Table 1, Table 2. Thus, there is no statistically significant difference between ELAs estimated using the AAR and AABR methods, (Table 2).

Table 1. ELA values for maximum glacial extent using a manual Accumulation Area Ratio (AAR) calculation and the Accumulation Area Balance Ratio (AABR) calculator in ArcGIS.

	ELA Calculation	
Glacier ID	**AAR (m)**	**AABR (m)**
KM_1	1960	1926
KM_2	1970	1989
KM_3	1940	1915
KM_4	1810	1825
KM_5	1970	2004
KM_6	2065	2085
KM_7	2000	2003
KM_8	1945	1933
KM_9	1990	1952

KM_10	2000	1993
KM_11	2005	1999

Table 2. Descriptive statistics for ELA estimates using AAR and AABR methods. Units are all listed in meters.

AAR		**AABR**	
Mean	1968.64	Mean	1965.82
Standard Error	18.99	Standard Error	20.16
Median	1970	Median	1989
Standard Deviation	62.97	Standard Deviation	66.85
Skewness	-1.48	Skewness	-0.47
Range	255	Range	260
Minimum	1810	Minimum	1825
Maximum	2065	Maximum	2085
Confidence Level (95.0%)	42.31	Confidence Level (95.0%)	44.91

4.2 Catchment analysis

The total size of the Blue Lake watershed is about 2.2 km^2. Sub-watershed 1 is the largest of the sub-watersheds (0.98 km^2, 44.5% of the total watershed), followed by sub-watershed 2 (0.32 km^2, 14.5% of total), and sub-watershed 3 (0.24 km^2, 11% of total; Figure 9). The remainder of the watershed covers 0.66 km^2 (30% of the total).

4.3 Blue Lake core analysis

4.3.1 Chronology

The age-depth model for core ABL16-LI has a projected basal mean calibrated age of 18,233 cal yr BP, with modern sediments at the top of the core (Table 3, Figure 10). This results in an average whole core sedimentation rate of 0.45 mm/yr. Between radiocarbon samples, calculated sedimentation rates are 0.58 mm/yr between 0 and 82 cm, 0.66 mm/yr between 82 and 124 cm, 0.47 mm/yr between 124 and 315 cm, 0.40 mm/yr between 315 and 700 cm, 0.41 mm/yr between 700 and 731 cm, and 0.49 mm/yr between 731 and 822 cm. The reservoir effect

determined from the average offset between paired macrofossil and bulk sediment ages at 82 and 315 cm depth is ~375 years.

Table 3. Depth in core and radiocarbon age of samples used to construct age-depth model and to calculate a reservoir effect (italicized). The calibrated age for samples 187493 and 186745 includes adjustments based on the calculated reservoir effect of 375 years. 2σ calibrated ages were calibrated with the dataset from Reimer *et al*. (2020).

Sample ID	**Lab ID**	**Depth (cm)**	**Material**	**^{14}C age (yr BP)**	**± yr (1σ)**	**Calibrated age ranges (2σ, yr BP)**			
						Min	**Max**	**Prob.**	**Median Prob.**
ABL16-LI-82-m	187322	82	Macrofossil	1575	35	1385	1531	1.000	1461
ABL16-LI-124-m	186744	124	Macrofossil	1365	45	1177 1218 1244	1214 1224 1350	0.207 0.009 0.784	1288
ABL16-LI-315-m	187323	315	Macrofossil	5310	80	5929 6231	6221 6278	0.906 0.094	6095
ABL16-LI-700-s	187493	700	Bulk sed.	12690	80	14840	15413	1.000	15127
ABL16-LI-731-s	186745	731	Bulk sed.	13260	40	15763	16076	1.000	15194
ABL16-LI-82-s	*187489*	*82*	*Bulk sed.*	*2005*	*30*	*1836* *1867*	*1854* *2001*	*0.035* *0.965*	*1941*
ABL16-LI-315-s	*187491*	*315*	*Bulk sed.*	*5600*	*35*	*6301*	*6446*	*1.000*	*6365*

4.3.2 Stratigraphic description

Core ABL16-LI contains a variety of sediments ranging from organic-rich gyttjas in the upper half of the core to predominantly low-organic siliciclastic laminated and poorly bedded intervals interspersed with higher-organic, poorly bedded intervals in the lower half. In general, clastic sediments in the core are dominated by silts, with subtle but notable changes in the concentrations of clay and sand between units. Organic content, magnetic susceptibility, and XRF scan data are highly variable and correspond to dramatic shifts in sedimentary composition, particularly in the lower half of the core. I divide core ABL16-LI into 12 stratigraphic units (Figure 11) based on sedimentary composition, grain size, organic content, and XRF elemental analyses (Figures 12, 13). There is no evidence of depositional hiatuses, bioturbation, or diagenesis.

Core ABL16-LI broadly contains an organic-rich, compositionally homogenous upper half (Unit 12) and a more variable, compositionally heterogenous lower half (Units 1–11; Figure 11). Unit 1 (746–822 cm) is a tan to brown finely-laminated silt with highly variable concentrations of sand (3–77%). The clay content in Unit 1 is low but highly variable (1-10%). Organic content is relatively low and highly variable (LOI 0.4–5%) and magnetic susceptibility is high and variable (1–11 SI x 10^{-5}). The bottom 25 cm contain several sequences containing graded sediments that transition from coarse to fine, including a notable sand-rich layer at 809 cm with a sharp basal contact with the sediments below transitioning into finer grained sediments above.

Unit 2 (728–746 cm) is a finely laminated brown silt with lower and less variable sand concentrations (1–9%) than Unit 1. The clay fraction in Unit 2 is relatively low (7–8%). Unit 1 gradually transitions into Unit 2, which has a higher organic content (LOI 5–10%) and lower magnetic susceptibility (1–5 SI x 10^{-5}) than Unit 1. Unit 2 has a sharp contact with Unit 3.

Unit 3 (709–728 cm) is a poorly bedded tan silt with minor clay (5–8%) and sand (1–9%) fractions. Unit 3 has a low organic content (LOI 2–3%) and a variable but relatively high magnetic susceptibility (3–9 SI x 10^{-5}). There is minor deformation from coring in Unit 3, but the original stratigraphy is mostly preserved. Unit 3 has a sharp contact with Unit 4.

Unit 4 (679–709 cm) is a brown finely laminated silt with infrequent mm- to cm- scale tan clastic-rich laminae. Clay (3–10%) and sand (3–21%) fractions are minor but variable. Organic content is relatively high and variable (LOI 7–13%), while magnetic susceptibility is mostly low (1–5 SI x 10^{-5}) with a minor peak of 8–9 SI x 10^{-5} in the thickest clastic-rich layer. Unit 4 has a diffuse contact with Unit 5.

Unit 5 (669–679 cm) is a light brown finely laminated silt with a relatively high clay (8–12%) fraction and a small sand (1–6%) fraction. Organic content is consistent (LOI 7–8%) and magnetic susceptibility is relatively low (2–4 SI x 10^{-5}). Unit 5 has a sharp contact with Unit 6.

Unit 6 (582–669 cm) is a tan silt with highly variable clay (3–10%) and sand (2–31%) fractions. Based on variable laminations throughout Unit 6, I have divided Unit 6 into three subunits. Unit 6a (648–669 cm) is mostly unlaminated, although there are infrequent minor laminations. Unit 6b (595–648 cm) contains mm- to cm- scale tan and gray laminations, although they are not as defined as the laminations in units 1 and 11. Unit 6c (582–595 cm) is unlaminated. Throughout Unit 6, organic content is consistently low (LOI 1–2%), while magnetic susceptibility is variable (2–7 SI x 10^{-5}). Grain size fluctuations are not clearly tied to transitions between subunits in Unit 6. Unit 6 and Unit 7 meet at a sharp contact.

Unit 7 (538–582 cm) is a dark brown laminated silt with variable clay fractions (4–8%) and variable sand fractions; the lower portion of the unit (564–582 cm) has a high sand component (8–25%), while the upper portion (538–564 cm) has a lower sand fraction of 2–9%. The unit has consistent organic content (LOI 5–7%) with a notable minimum of 1% in a clastic-rich horizon at 564 cm. Magnetic susceptibility in Unit 7 is relatively consistent and low (0–2.5 SI x 10^{-5}). Unit 7 has a diffuse contact with Unit 8.

Unit 8 (529–538 cm) is a massive brown silt with minor clay (7–8%) sand (4–7%) fraction. Organic content is consistent (LOI 6–8%), and magnetic susceptibility ranges from 0.3–2 SI x 10^{-5}. Unit 8 has a sharp contact with Unit 9.

Unit 9 (508–529 cm) is a dark brown silt with infrequent mm-scale laminae. The sand fraction is minor (2–5%) apart from two peaks of 9%, and the clay fraction is slightly higher than

Unit 8 (7–10%). LOI is relatively high (8–11%) and magnetic susceptibility is low, ranging from 0–1 SI x 10^{-5}. Unit 9 has a diffuse contact with Unit 10.

Unit 10 (487–508 cm) is a massive tan silt with minor clay (7–10%) and sand (4–8%) fractions. LOI increases from 5% at the base of the unit to 8% at the top. Magnetic susceptibility is consistent, varying from 1–2.5 SI x 10^{-5}. Units 10 and 11 share a sharp contact.

Unit 11 (462–487 cm) is a laminated tan to brown silt with a substantial sand fraction (13–48%) in the bottom 4 cm. This sand-rich interval closely resembles the graded sediment packages identified in Unit 1. Grain size is quite variable in the rest of the unit, with the clay fraction ranging from 5–11% and the sand fraction ranging from 0–18%. LOI is somewhat variable as well (3–8%), while magnetic susceptibility varies from 0–3 SI x 10^{-5}.

Unit 12 (0–462 cm) is a dark brown, poorly bedded, organic-rich silt encompassing the top half of the core. Overall, Unit 12 is overwhelmingly silt-dominated, although there is considerable variability in clay (4–16%) and sand (1–10%). Additionally, the sediments comprising Unit 12 are the most organic-rich in the core, with LOI varying from 18–31%. Terrestrial plant macrofossils are abundant throughout Unit 12. Magnetic susceptibility is low with some variability (-0.5–2.5 SI x 10^{-5}). Subtle but notable differences within Unit 12 support subdividing the unit into five subunits; Unit 12a (408–462 cm), Unit 12b (400–408 cm), Unit 12c (130–400 cm), Unit 12d (71–130 cm), and Unit 12e (0–71 cm). During the extended core curation at ANSTO, select intervals in Unit 12 have experienced substantial water loss; data from these intervals are excluded from this report. Units 12a, 12c, and 12e all have high organic contents (> 24%) and lower concentrations of sand (< 8%). Unit 12b is substantially less organic rich (LOI 9–13%) and contains high sand concentrations (10–34%). Unit 12d has slightly lower organic content than units 12a, 12c, and 12e (18–21%) along with slightly higher magnetic

susceptibility (Figure 8). The contacts between the subunits of Unit 12 are diffuse and difficult to discern in the visual stratigraphy except for a fairly sharp contact between units 12b and 12c.

I recognize four lithofacies in core ABL16-LI. These are: 1) organic-rich (>18% LOI) massive silts with abundant macrofossils (Unit 12); 2) medium to dark brown silts, often laminated, with LOI values between 8–13% with relatively little variability in grain size (units 2, 4, 5, 8, and 9), with a related facies (termed Facies 2a) with similar overall characteristics but lower overall average LOI values of about 5% (Unit 7); 3) unbedded to slightly laminated, clastic-rich (LOI <8%) silts with variable grain size, relatively high sand fractions (>8%), and relatively high magnetic susceptibility (>3 SI x 10^{-5}) (units 3, 6, and 10); and 4) highly variable, clastic-rich silts (LOI <8%) containing mm- to cm- scale laminae (units 1 and 11).

4.3.3 Xray fluorescence

Elemental ratios for K/Zr, Zr/Rb, Si/Ti, K/Ti, and log(Rb/Sr) are variable throughout core ABL16-LI (Figure 13). The primary XRF grain-size proxies (K/Zr, Zr/Rb, and Si/Ti) all show high variability prior to about 9.7 cal ky BP, with subtler fluctuations through the Holocene. K/Zr and Zr/Rb show a partial anti-phase relationship, where apposing maxima and minima in either proxy often occur simultaneously. K/Zr is generally higher, though variable, before about 9.7 cal ky BP, where it experiences low values until the late Holocene (around 2.2 cal ky BP). Zr/Rb is highly variable throughout the deglacial period but does not experience an increase that might be expected given its relationship to K/Zr lower in the core. Si/Ti shows a mildly similar trend to Zr/Rb, although its variability is lower. Si/Ti has a large maximum at 18.0 cal ky BP, followed by a drastic decrease that persists until the contact of units 5 and 6 at 14.9 cal ky BP. Si/Ti remains high but variable throughout Unit 6, and rapidly decreases at 12.2 cal ky BP.

Above that sudden change, Si/Ti consistently decreases until about 9.7 cal ky BP, where it remains low with little variability throughout the Holocene.

The two ratios used to reconstruct weathering (K/Ti and log(Rb/Sr)) show overall similar trends with high values (aka, lower weathering rates) between 18.2 and 9.1 cal ky BP and low values (higher weathering rates) after 9.1 cal ky BP (Figure 13). The highest value for K/Ti is at the base of the core, with values consistently decreasing upwards until about 14.9 cal ky BP, where there is a rapid increase at the contact of units 5 and 6. High K/Ti values (reduced physical weathering) are sustained until about 12.6 cal ky BP, at which level there is a gradual upward decrease into a steady state of low values at about 9.1 cal ky BP. K/Ti is low (high physical weathering) with some minor variability throughout the Holocene, with a notable increase in unit 12d between about 2.2 and 1.2 cal ky BP. Log(Rb/Sr) shows a similar trend in the bottom half of the core, with a peak at the base followed by a slightly lower steady state until about 15.3 cal ky BP, where there is a sharp decrease followed by increase at 14.9 cal ky BP. Log(Rb/Sr) values are then mostly consistent with some variability until about 9.1 cal ky BP, where they reach a minimum. Log(Rb/Sr) values then slowly increase throughout the remainder of the Holocene until they reach a peak at about 1.3 cal ky BP, similar to K/Ti.

5. Discussion

5.1 LGM glacier reconstructions

5.1.1 Glacial mapping

Because there are relatively few glacial landforms visible in the lidar bare-earth imagery, determining the exact extents of some glaciers was difficult. Several former glaciers have obvious visible landforms in their former ice extents – for example, the KM_9 glacier ice extent includes several moraines, flutes, cirque walls, and a glacial tarn lake (Figure 5). Others,

however, have fewer glacial landforms in their former ice extents, such as KM_1 and KM_2, which appear to have cirque features in their accumulation zones, but no indicators of ice flow or moraines in their lower reaches. Thus, because of the subtle nature of the Snowy Mountains' glacial landforms, the maximum ice extents of some glaciers are difficult to reconstruct, which introduces some uncertainty in regional ELA estimates.

My remapping indicates that the maximum glacial extents on the Kosciuszko Massif were likely somewhat larger than those mapped by Barrows *et al*. (2001). Several trends are evident that explain many of the differences in specific cirques. For example, Barrows *et al*. (2001) mapped the upper extents of several glaciers as being smaller (i.e., at a lower elevation) than in my mapping because of their lower-resolution map base (see glacier KM_3, Figure 7). I also did not identify glacial landforms in the eastern extent of the KM_8 glacier consistent with the mapping by Barrows *et al*. (2001). Additionally, I expanded the area of maximum ice extent for several glaciers, particularly KM_5 and KM_7. In the case of KM_5, it appears that the stream at the base of my mapped ice extent is diverting around a deposit that is not susceptible to erosion, which may be a glacial deposit (Figure 7). Field observation of this site would be necessary to confirm this inference. Additionally, in the case of the KM_7 glacier, I determined that the accumulation area of the glacier was larger due to cirque features south of the area mapped by Barrows *et al*. (2001). Overall, however, these differences are relatively minor and do not dramatically change the average ELAs or climatic conditions that can be inferred from the glaciers (cf., Galloway, 1965).

5.1.2 Equilibrium line altitude estimates

Equilibrium line altitudes during the maximum glacial extents are quite variable (Table 1, Table 2, Figure 8). Even in the highest altitudes of the Snowy Mountains, much of the land surface was not glaciated, even during maximum glacial extents. This indicates that the regional ELA remained above the highest altitudes even during maximum glacial conditions, and certain locations that were favorable to the formation of glaciers at lower altitudes due to local orographic effects and snow drifting, much like in the modern Sierra Nevada (e.g., Gillespie and Clark, 2011). For example, south facing slopes receive far less sunlight than north facing slopes, and would experience less ablation, while east facing slopes would have increased accumulation due to snow drifting from westerly winds. This might explain why some ELAs are quite low, such as the KM_4 glacier, which would have had south and east facing cirque walls. In the case of north facing glaciers, such as KM_11, the ELA is much higher, and there are some sections of the accumulation area that are east facing and would have had a large snow drift input. There were no west facing glaciers in the Snowy Mountains, which suggests that snow drifting was a major driving factor in promoting sufficient snow accumulation to allow for the formation of flowing ice.

The two methods I used in this study do not produce statistically significant differences in average ELA estimates. However, for individual glaciers, there are differences between the AAR and AABR estimates (KM_1, KM_5, and KM_9, see Table 2). Some of these differences may arise from the difficulty in manually creating AAR ELA estimates. For some glaciers, the area of the accumulation area can shift substantially if one side of the glacier had a less steep slope gradient than the other. Thus, changes in the ELA of even a few meters can drastically change the apparent size of the accumulation area. Additionally, there is uncertainty regarding the ratios

I used in both methods. There are no published accumulation area or accumulation area balance ratios for Australia. The well-established values for the Cascade Mountains in Washington State, USA (Rea, 2009), that I use in this study may not fully reflect the conditions that were present when the Snowy Mountains were glaciated.

5.2 Chronology

The age model for core ABL16-LI is the most parsimonious result based on several simulations using different combinations of ^{14}C samples, confidence intervals, and contacts between units that are interpreted as depositional hiatuses (Appendix A). In the final version, several bulk-sediment samples were omitted because they were anomalous, and the Bacon algorithm ignored them during its simulations. These anomalous dates also require unreasonable sedimentation rates given the well-bedded character of the stratigraphy and the relative stability of the landscape surrounding Blue Lake. In this discussion, I focus solely on the single best age-model (Figure 10); Appendix A contains a more detailed discussion of the other potential age models and of the age-model selection criteria.

There are a few aspects of the final age-depth model that necessitate further discussion. The plant macrofossil samples in the uppermost portion of the core (at 82 cm and 124 cm depth) have inverted ^{14}C ages, even accounting for analytic uncertainties (Table 3; Figure 10). This is reflected in the age-depth model (Figure 10) and the observed sedimentation rates between samples, where Bacon interpolates the highest sedimentation rate (0.66 mm/yr) in the whole core between these samples in order to accommodate the age inversion. The age-depth model is entirely influenced by the 82 cm date, where the difference between the modeled age and the calibrated age is 43 years compared to 768 years for the 124 cm date. In general, it is difficult to justify removing a plant macrofossil date from an age model because they are generally the most

reliable material for AMS dating of sediment cores. It is possible that the 82 cm sample could appear erroneously old if it is from material that was stored in the catchment soil before being deposited in the lake. Alternatively, bioturbation could have transported the 124 cm sample down in the sediments and produced an erroneously young age. Neither of these options seems particularly reasonable for this core, so I determined that it was not justifiable to remove either date from the age-depth model. As a result of this uncertainty, the timing of any environmental changes in the upper ~1.3 m of the core remains less certain.

Another concern of this age-depth model is the use of bulk sediment dates in the basal 1.2 m of the core. The use of bulk sediment dates in age-depth models is sometimes contentious because reservoir effects can vary from 500 to 2000 years (Grimm *et al*., 2009). Bulk sediment samples can potentially contain coal or lacustrine plant matter containing carbon that is sourced from bedrock or soil (Grimm *et al*., 2009). Therefore, I prioritized obtaining terrestrial macrofossils during the sampling process because they get their carbon directly from the atmosphere during photosynthesis. Such samples were more common in the upper half of the core (Unit 1), but rare in the lower half of the core. I collected samples that were slightly larger than the minimum size (~0.3 mg) at 476, 700 and 731 cm depth, but after pretreatment, these samples did not produce enough carbon to obtain a reliable AMS analysis. Therefore, I needed to rely on several bulk organic analyses to supplement the two viable macrofossil analyses. In order to constrain the reservoir effect for the bulk samples, I analyzed bulk sediments adjacent to the macrofossil samples. This provided greater confidence in the bulk sediment analyses from the base of the core, but because of the higher uncertainty associated with bulk sediment dates, the timing of environmental changes in the lower portion of the core are less certain than the upper part of the core. Further lake sediment studies within this broader project should focus on

obtaining high-quality plant macrofossils for AMS dating in the lower portions of their sedimentary sequences. Chronologies including such samples will reduce some of the temporal uncertainty associated with this study and interpret the timing of major environmental changes with more confidence.

5.3 Sediment facies and depositional interpretations

The establishment of lithofacies is important in developing environmental interpretations from lake sediments. In this section, I discuss the characteristics of each lithofacies and the environmental conditions that could lead to their deposition.

Facies 1 (Unit 12, 9.7 cal ky BP – present) composes the upper half of the core and contains the most organic-rich sediments in the core. Grain size is silt-dominated but there are variable and sometimes substantial clay and sand fractions; however, grain size variability is relatively low in Facies 1 as recorded by its SPAN values (Figure 12). Variability in magnetic susceptibility and weathering proxies (Figures 12, 13) are also low. In combination, these trends suggest a relatively stable environment throughout this facies with a vegetated and productive catchment. Few sand beds suggest lower energy streamflow and minimal direct transport of sediment into the lake from local slopes. Low magnetic susceptibility also strongly suggests that minerogenic input into the lake is low in Facies 1. I interpret Facies 1 as being deposited during intervals of relatively warm and humid climate, likely somewhat similar to the modern climate of the Snowy Mountains (Figure 3).

Diatoms observed in smear slides of Facies 1 sediments suggest that primary productivity is present in the lake during the deposition of this facies. However, allochthonous organic matter is substantially more abundant than diatoms and qualitatively suggests that while there are

contributions of both terrestrially and aquatically sourced organic matter in these sediments, the terrestrial fraction dominates. Additionally, other macroscopic primary producers such as moss and algae were not observed in any of the sediments in Facies 1. Moreover, Blue Lake is presently oligotrophic and is therefore unlikely to have had a large amount of primary productivity during the rest of the Holocene. The most likely period for the development of eutrophic conditions that are more conducive to primary productivity would be during the 19th through 21st centuries when cattle grazing occurred even in the highest portions of the Snowy Mountains (Australian Alps National Parks, 2013), but it appears that Blue Lake remained oligotrophic. Without more specific data such as C/N ratios from organic matter (e.g., Perdue and Koprivnjak, 2007), the exact contributions of terrestrial vs. aquatic organic matter are unresolved, but available evidence indicates that much of the organic matter in the lake sediments is sourced from vegetation in the catchment.

Facies 2 (units 2, 4, 5, 8, and 9) is analogous to Facies 1 but has lower LOI values, typically by 10 to 20%. Much like Facies 1, Facies 2 has consistent grain size with notably low sand concentrations and consistently low magnetic susceptibility values (Figure 12). Facies 2 sediments mostly contain laminated sediments that are evident both in visual and X-radiographic core images (Figure 11). The compositions of individual laminae vary, with some being defined by color differences (i.e., medium to dark brown presumably resulting from mm-scale organic content variations) and composition, where select laminae are virtually devoid of organic matter and appear similar to clastic-rich horizons in facies 3 and 4. The units comprising Facies 2 occur in the bottom half of the core, and I interpret them as warm and wet relative to the units that surround them from facies 3 and 4, but cooler and/or drier than Facies 1 (i.e., reduced vegetation productivity in the catchment). I suggest this difference between facies 1 and 2 because the

organic content is so much lower in Facies 2, and because it contains to cm- scale clastic rich horizons that might represent sudden slope destabilization or brief intervals with less vegetation in the catchment.

Facies 2a (Unit 7) is similar to the rest of Facies 2 but with a lower LOI value that falls almost exactly between Facies 2 and facies 3 and 4. I posit that the climatic conditions contributing to the deposition of Facies 2a are similar to Facies 2 but may have been slightly colder and/or drier, but not to the point that vegetation was not established in the catchment. Based on the LOI and indicators of clastic sediment input, this facies still appears much more similar to Facies 2 than any other facies, and still represents relatively warmer and/or wetter conditions in the context of deglacial climate.

Facies 3 (units 3, 6, and 10) contains clastic rich sediments with variable grain size, high but variable magnetic susceptibility and low organic content. The degree of lamination is low but variable in this facies; for example, Unit 6b contains mm- to cm-scale gray and tan laminations but is otherwise similar to the rest of the facies in its sedimentologic characteristics. The most unifying characteristic of Facies 2 is a low organic content, which is complemented by a lack of identifiable plant macrofossils. During the deposition of Facies 3 units, the catchment appears to have been almost entirely devoid of vegetation. This likely results from cold or dry climate conditions that are not conducive to vegetation and/or persistent snow cover that substantially limited vegetation growth. This situation could potentially signify the presence of small glaciers or permanent snowfields following the LGM, but there is no geomorphic evidence for glaciers after 15.9 ka (Barrows *et al.*, 2001). Grain size, weathering, and magnetic susceptibility proxies are all highly variable throughout Facies 3 (Figures 12, 13). Clay content is relatively stable throughout the facies, but there are notable differences between the relative proportions of silt

and sand. These shifts are on the scale of tens of centimeters rather than distinct beds, and therefore mostly represent a change in overall catchment conditions instead of discrete events; however, there are a select few sharp peaks in sand concentration that likely result from discrete depositional events. In general, larger grain size distributions should reflect higher energy within the lake system. Increased energy in the lake might result from increased streamflow, a lowering of the lake level resulting from a decrease in the precipitation/evaporation ratio, or changes in slope weathering conditions.

Facies 4 (units 1 and 11) contains highly laminated silts with predominantly low organic content and large variability in the other paleoenvironmental proxies. The mm-scale laminae in this section reflect rapidly changing patterns of deposition, and there are clear visual shifts in organic content and grain size to complement the heightened variability in paleoenvironmental proxies (Figures 12, 13). Grain size shifts predominantly reflect fluctuations in the relative fractions of sand and silt. Although silt is far more abundant in these sediments, the presence of sand-rich intervals indicates increased energy in the lake. The inferred causal mechanisms for this increased energy in the lake system are the same as in Facies 3. Sparsely distributed sub-mm-scale organic-rich laminae might represent brief periods of wetter conditions that allowed for increased productivity within the catchment. They might alternatively result from periods with warmer summer temperatures that promoted greater vegetation growth.

The packages of graded sediments in Facies 4 are of particular interest. They consist of mm- to cm-scale sand horizons with a graded basal contact and upward-fining sequences immediately above them that appear to have been deposited in a single event; these sequences closely resemble turbidites described by Howarth *et al.* (2021). In order to reasonably interpret these sequences as turbidites, both a sediment source and triggering mechanism are necessary.

These sequences are most common in intervals with very low organic content and no macroscopic terrestrial plant fossils, suggesting that the catchment was at least partially devegetated. The fan-delta deposit on the western shore of Blue Lake (Figure 9), which is presently vegetated, is fed by the largest sub-basin in the Blue Lake catchment and would have been more susceptible to periodic failures that could release sand- and smaller-sized particles deeper into the lake basin. Pulses of snow- or glacial-meltwater or heavy summer precipitation could have been large enough and transported enough sediment to destabilize the submerged fan-delta foresets and create turbidites that flowed into the deeper lake basin.

5.4 Deglacial and Holocene environmental interpretations

In this section, I discuss inferred climatic and environmental changes from proxy data at Blue Lake over the last ~18.2 cal ky BP. All ages reported in this section are mean dates based on the age-depth model for core ABL16-LI (Figure 10). Where relevant, the I also discuss the 2-σ confidence interval for the ages of transitions.

5.4.1 Early deglacial period (18.2 – 14.9 cal ky BP)

Sediments from the early deglacial period are highly variable in their visual characteristics and in proxy data, suggesting that repeated episodes of rapid environmental change occurred immediately following deglaciation. Unit 1 (18.2 – 16.7 cal ky BP) was deposited after the formation of the lake and contains highly variable organic-poor laminated sediments. These sediments contain several sediment packages containing 0.5 – 1 cm beds of sand, which I interpret as lacustrine turbidites. The presence of these turbidites suggests that the Blue Lake catchment was delivering sediment to the lake in discrete events. The most likely

source for such sediment pulses is the western delta (Figure 9), which likely periodically failed and delivered sediment to the lake floor. To facilitate this discrete sediment delivery, the catchment likely would have been largely free of vegetation, which is reflected in low LOI values (Figure 12). Although several turbidite packages have been identified in Unit 1, other horizons have low sand concentrations and appear to reflect more gradual background deposition from the catchment. These non-turbidite sediments are laminated but do not show a predictable rhythmic pattern as would be expected in varves and are thus do not appear to be true (annual) varves. Clastic varves commonly found in alpine and proglacial lakes are typically marked by coarse-grained lamina capped by distinct clay laminae (Zolitschka *et al*., 2015). The laminae in the Blue Lake core do not match this description (Figure 12). Thus, background sedimentation predominantly through physical weathering appears to be an important process in the deposition of Unit 1 but does not carry a definitive seasonal signal.

Unit 1 has low LOI, high and variable magnetic susceptibility, variable grain size with an overall high sand fraction, and high log(Rb/Sr) and K/Ti values (low weathering) (Figures 12, 13). This suggests a cold/and or dry climate immediately following deglaciation. The presence of thin (≤ 1 mm) dark organic rich laminae in conjunction with a slight increase in LOI and decrease in magnetic susceptibility (Figure 12) suggests that vegetation was slightly increased in the catchment towards the end of Unit 1 deposition.

There is a sharp change in many of the proxy data at the contact of units 1 and 2 (at 16.8 cal ky BP). Unit 2 (16.7 – 16.3 cal ky BP), deposited under Facies 2 conditions, has a nearly 10% increase in LOI, low but variable magnetic susceptibility, and less variable grain size with a lower overall proportion of sand (Figure 12). There are also dramatic decreases in log(Rb/Sr) and K/Ti that both suggest an increase in chemical weathering in the catchment (Figure 13).

Combined, these proxies suggest that a vegetation community was established in the catchment, likely under warmer and/or wetter conditions.

The brief climate amelioration that occurred during the deposition of Unit 2 was reversed with the deposition of Unit 3 (16.3 – 15.8 cal ky BP). Unit 3 was deposited under Facies 3 conditions, with low LOI and high magnetic susceptibility (Figure 11). The grain size distribution, Si/Ti, and Zr/Rb show a relatively low overall sand content, and SPAN suggests that grain size variability is low (Figures 12, 13). Log(Rb/Sr) and K/Ti are both high, signaling reduced weathering, especially chemical weathering (Figures 12). These data suggest cool and/or dry conditions, but with a fundamentally different environment than that of Unit 1.

The end of the deglacial period was marked by another brief climate amelioration during the deposition of units 4 and 5 (15.8 – 14.9 cal ky BP). Units 4 and 5 (Facies 2) have similar characteristics to Unit 2, with high LOI, low magnetic susceptibility, and relatively high chemical weathering rates inferred from log(Rb/Sr) and K/Ti (Figures 12, 13). The grain size in these units is less variable and contains a smaller sand fraction than Unit 2 (Figure 12). The environmental interpretation for this interval is similar to that of Unit 2, with conditions ameliorating into a warmer and/or wetter climate that fostered the re-establishment of a vegetation community in the Blue Lake catchment.

5.4.1.1 Regional context for the early deglacial period

According to the age-depth model in this study, the base of the Blue Lake core dates to ca. 18.2 cal ky BP (95% confidence interval: 19.0 – 17.6 cal ky BP). This generally agrees with the timing for the onset of deglaciation suggested by Barrows *et al*. (2001), who found that deglaciation likely began before 18 ka. The timing of deglaciation across the Southern

Hemisphere is largely consistent with these dates, as it was ca. 19 ka in Antarctica (Pedro *et al*., 2011) and between 21 – 18 ka in New Zealand (Shulmeister *et al*., 2019).

Other records from the Trans-Australian region suggest that the early deglacial period had a highly variable climate. At North Stradbroke Island (Figure 6), mean February temperatures rose 3 ºC between 18.1 and 17.3 ka (Chang *et al.*, 2015). From 18 to 15 ka, Southern Ocean sea ice retreated, and sea surface temperatures rapidly rose to Holocene levels (Barrows *et al.*, 2007; Reeves *et al.*, 2013). Existing lake-level records from the early deglacial period (18-15 ka) at Lake Frome and Lake Eyre to the west-northwest of KNP suggest spatially variable humid and arid conditions, although the sites used for these studies are distant from KNP (Figure 6; De Deckker *et al*., 2011; Reeves *et al.*, 2013). These rapid fluctuations may correspond to deposition of Unit 2 (16.7 – 16.3 cal ky BP) and units 4 and 5 (15.8 – 14.9 cal ky BP). It is not necessarily problematic that the timing does not completely align, as the broad range of possible ages in the 95% confidence interval of the age-depth model (Figure 10) leave considerable leeway in the timing of these units. It is clear from the Blue Lake that the period ~3,000 years immediately after the lake was formed were characterized by millennial to sub-millennial-scale climatic and environmental change.

5.4.2 Antarctic Cold Reversal (14.9 – 12.6 cal ky BP)

There appears to be good evidence for cooling at Blue Lake coincident with the Antarctic Cold Reversal. Unit 6 (Facies 3; 14.9 – 12.6 cal ky BP) overlaps with the timing of the ACR (14.7 – 13.0 ka, Pedro *et al*., 2016) within the dating uncertainties. At Blue Lake, this period is defined by extremely low organic deposition as recorded by LOI and relatively high-energy deposition in the lake as indicated by grain size, Si/Ti, and Zr Rb (Figures 12, 13). The sediment visually appears almost entirely clastic and has high magnetic susceptibility (Figures 11, 12).

Together, these proxies suggest that the catchment had little vegetation, and that deposition in the lake was largely restricted to sediment from the catchment and aeolian dust. To restrict vegetation in the catchment, climate would have been cooler and/or drier. Pedro *et al.* (2016) performed an analysis of ACR climate records across the Trans-Australian region suggesting that regions south of 40º S likely experienced 1–2 ºC of cooling but little to no change in precipitation. In southeast Australia, their simulation predicts 0–1 ºC of cooling; the magnitude of sedimentologic change coincident with the ACR at Blue Lake suggests that cooling was possibly larger, but this study does not provide quantitative constraints on temperature. Overall, the results from Pedro *et al.* (2016) suggest that changes in temperature were more substantial than changes in precipitation during the ACR. Their simulation indicates minimal change in precipitation in southeast Australia, suggesting temperature was the primary climate shift driving the shift in sedimentation at Blue Lake. It will take analyses that are beyond the scope of this study (e.g., chironomid palaeothermometry or leaf wax hydrogen isotopes to reconstruct precipitation), to confirm this inference. Nonetheless, the ACR appears to have impacted the environment of the Snowy Mountains.

The evidence at Blue Lake for an ACR signal agrees with emerging evidence that southeast Australia experienced at least some degree of cooling between about 14.7 – 13.0 ka. Petherick *et al*. (2009) report cool and arid conditions at North Stradbroke Island (Figure 6) coincident with the ACR. Pollen evidence from Paddy's Lake in Tasmania (Figure 6) records the presence of non-arboreal taxa, which reflects cooling (Beck *et al*., 2017). There is also evidence of reduced fire in portions of southeast Australia coincident with the timing of the ACR (Mooney *et al*., 2011) inferred to reflect cooler temperatures that restricted the growth of vegetation. Records from New Zealand and offshore southern Australia also suggest cooling during the ACR

(Calvo *et al*., 2007; Williams *et al*., 2009), but studies disagree on whether there were glacial advances in New Zealand (e.g., Williams *et al*., 2009; Putnam *et al*., 2010). There is evidence for glacial advance during the ACR in central Patagonia (Mendelová *et al*., 2020), and at the high-southern latitude island of South Georgia (Graham *et al*., 2017), which suggest that glacier expansion occurred during this interval. This is unlikely to have been the case in the Snowy Mountains, however, because there is no evidence of post-LGM glaciation at this site. Recent work has suggested that the ACR resulted from a reorganization of oceanic and atmospheric circulation that regionally included changes in atmospheric CO_2, which was driven by a northern shift in the southern westerly winds (Fletcher *et al*., 2021). This shift was observed by Fletcher *et al*. (2001) in Tasmania, but to account for the environmental changes observed at Blue Lake, it is possible that this shift extended further north towards the southern Australian mainland. Quantitative temperature reconstructions from the lakes in the Snowy Mountains would provide an important test of this hypothesis. Overall, Blue Lake appears to be in general agreement with sites in the trans-Australian region in that there was cooling during the ACR period.

5.4.3 Younger Dryas period (12.6 – 10.8 cal ky BP)

Based on the age-depth model for core ABL16-LI, there is evidence for relatively warm and wet conditions during the Younger Dryas period (12.9 – 11.7 ka; Rasmussen *et al*., 2006). Units 7, 8, and 9 (facies 2 and 2a) correspond to the YD period. These facies are characterized by relatively high organic content and low magnetic susceptibility, although grain size variability as shown by grain size data, median grain size, SPAN, Zr/Rb, and K/Zr is high through these units (Figures 12, 13). The change in LOI is particularly dramatic with an increase from around 1% in unit 6c (late ACR) to between 5% and 8% in units 7, 8, and 9 (Figure 12). The weathering

proxies are somewhat decoupled during this period, as log(Rb/Sr) does not indicate an increase in weathering, but K/Ti suggests that the rate of chemical weathering was increased (Figure 13). Overall, the proxies show a reversal from cool/dry ACR-like conditions to warmer and/or wetter conditions between 12.6 and 10.8 cal ky BP. The contact between units 6 and 7 is sharp, indicating that the shift from cooler/drier conditions to warmer/ wetter conditions was rapid. Higher LOI after the ACR suggests that vegetation was able to re-establish itself in the catchment, although the presence of occasional clastic-rich lamina suggest that sediment pulses still entered the lake, most likely in discrete depositional events. One particular horizon in Unit 7 is a 1-cm thick clastic bed that is coarse-grained (~30% sand) grading into a finer, but still-clastic rich sedimentary sequence; this bed is similar to the turbidite horizons discussed in section 5.2. The presence of this horizon in combination with the otherwise relatively organic-rich beds suggests that the vegetation communities may have been somewhat unstable or spatially discontinuous, which might reflect climatic instability or a complex ecosystem response after the ACR.

Other studies in the Trans-Australian region have provided contrasting evidence regarding the presence of the Younger Dryas, leaving its spatial extent unresolved. Some studies indicate that Australia experienced cooling during the YD. For example, Goede *et al*. (1996) report evidence of a –2 ºC temperature anomaly from a Royal Cave speleothem in eastern Victoria between 12.3 – 11.4 ka. Moreover, there is evidence from marine sediments off the south coast of Australia that suggests cooling during the YD, although it was dampened compared to those in the Northern Hemisphere (Andres *et al*., 2003). Elsewhere in the Southern Hemisphere, there is additional evidence of cooler conditions during the YD. In the North

Patagonian Icefield, glaciers were at their largest post-LGM extents during the YD (Glasser *et al*., 2012).

Contrastingly, proxy records from other sites in the Trans-Australian region do not show evidence of the YD. For example, on the South Island of New Zealand, conditions were warm and dry and there is no evidence for glacial advances at that time (e.g., Reasoner *et al*., 1994; Barrows *et al*., 2007; García-Ruiz *et al*., 2012; Hinojosa *et al*., 2019). Sea surface temperature reconstructions off the southern coast of New Zealand also indicate that locally, the Southern Ocean warmed during the Younger Dryas (Barrows *et al*., 2007). A review of the Younger Dryas in Australia also found no convincing evidence for cooling at that time, but also noted the general paucity of records covering the period (Tibby, 2012). Additionally, the ^{10}Be exposure dates on moraine boulders that form the basis for the conclusion of a YD signal in Patagonia by Glasser *et al*. (2012) have been challenged because the boulders were likely submerged in a lake for some time after they were deposited (Thorndycraft *et al*., 2019); dates of maximum ice extents at other nearby sites align more closely with the timing of the ACR (e.g., Sagredo *et al*., 2018).

With the caveat that records are somewhat sparse, the Blue Lake record appears to align more closely with studies suggesting no regional Younger Dryas cooling as well as the emerging conceptual model of general warming in the Southern Hemisphere during the YD (e.g., Kaplan *et al*., 2010). If the latter case proves valid, it would indicate an extreme thermal gradient between the Northern and Southern hemispheres during the YD. Such a gradient could be explained as a response to weakening of the Atlantic Meridional Overturning Circulation, which would have reduced heat transport between the Northern and Southern hemispheres (e.g., Kaplan *et al*., 2010). The evidence for relatively warm and/or wet conditions at Blue Lake during the

Younger Dryas suggests that Blue Lake was in the "warmer" portion of this gradient. At present, this record suggests but does not confirm this; a quantitative temperature reconstruction will confirm whether this is the case.

5.4.4 Earliest Holocene (10.8 – 9.7 cal ky BP)

Immediately following the warmer and/or wetter conditions signified by units 7, 8, and 9, a final clastic-rich sedimentary sequence was deposited between 10.8 – 9.7 cal ky BP (units 10 and 11). Unit 10 is classified as Facies 3 while Unit 11 is classified as Facies 4 primarily due to the presence of laminae in Unit 11. Unit 10 has low organic content (LOI 2–6%) and magnetic susceptibility ranging between 1 – 3 SI x 10^{-5}, which is lower than the clastic-rich units lower in the core, but higher than the more organic-rich units above and below (Figure 12). Unit 10 has a relatively uniform grain size distribution with a relatively low sand fraction and relatively low values for log(Rb/Sr) and K/Ti, suggesting increased chemical weathering (Figures 12, 13). Unit 11 on the other hand has a similarly low organic content and similar magnetic susceptibility values but a much higher degree of grain-size variability (Figure 12), including several distinctive sand-rich horizons that mimic those observed in Unit 1. Log(Rb/Sr) and K/Ti are also higher in Unit 11, suggesting reduced weathering (Figure 13). In conjunction, the low organic content of these units suggests that vegetation cover was substantially reduced in the Blue Lake catchment, but other proxies show conflicting responses that make environmental interpretation more complicated than for other intervals.

While these units signify a major environmental change at Blue Lake, similar deposits have not been identified over this period at other sites in Australia or the Trans-Australia region. Results from Little Llangothlin Lagoon (Figure 6), another cool, high-altitude site in Australia,

show no evidence of this reversal as climate conditions were relatively warm and wet by 11.7 ka (Ellerton *et al*., 2017). Indeed, other studies from elsewhere Australia suggest that the early Holocene (beginning around 12 ka) was warm and wet (e.g., Kershaw *et al.*, 2007; Petherick *et al.*, 2013; Wilkins *et al.*, 2013). There is no evidence for changes in fire regimes in Australia that might correspond with these units; these changes are inferred to be primarily controlled by climate prior to the late Holocene (Mooney *et al*., 2011). If the deposition of these units is purely climate related, this lack of evidence elsewhere suggests that the effects may have been experienced on a small scale in the Snowy Mountains. Units 10 and 11 are also far from radiocarbon ages, making this one of the least temporally constrained intervals in the core. The 95% confidence interval in the age-depth model indicates that this interval could have started between 11.7 – 9.9 cal ky BP and ended between 10.6 – 8.9 cal ky BP (Figure 10). Therefore, within uncertainty, this interval could possibly correspond to the later stages of the YD, in which case there would be evidence for cooling and/or drying during that interval. Of the depositional regimes observed in Blue Lake, units 10 and 11 are the most difficult to interpret. Records from the other lakes in the Snowy Mountains may help to resolve if these units are a regional climatic event or perhaps a localized depositional event specific to the catchment.

5.4.5 Early and mid-Holocene (9.7 – 2.2 cal ky BP)

After 9.7 cal ky BP, the record dramatically shifts into Facies 1, in which sediments have high organic content, low magnetic susceptibility, relatively stable and sand-poor grain size assemblages, and low values for log (Rb/Sr) and K/Ti indicating substantial weathering (Figures 12, 13). Facies 1 is generally interpreted to indicate a productive vegetation community in the catchment fostered by a relatively warm and wet climate with conditions similar to those

presently found at the lake. Clastic sediment deposition is lower throughout this unit, which suggests more stable slopes resulting from substantial vegetation coverage of the catchment. Many of the measurements and proxies, particularly grain size, are relatively stable throughout this entire interval, suggesting that the environment was similarly stable throughout much of the Holocene. There are two notable departures from these conditions marked by units 12b and 12d, which are discussed in the following two sections.

During much of the Holocene, the Blue Lake record appears to be consistent with other Australian environmental records. Sea surface temperatures in the Southern Ocean were equivalent to modern by the early Holocene (Barrows and Juggins, 2005). High lake levels, increases in rainforest taxa, increased fluvial discharge, and a rapid increase in the abundance of *Eucalyptus* pollen at higher altitudes indicate that the early Holocene (designated globally from 11.7 to 8.2 ka, Walker *et al*., 2018) was relatively warm and wet in much of southeastern Australia (Kershaw *et al.*, 2007; Petherick *et al.*, 2013; Wilkins *et al.*, 2013). The early Holocene is also marked by an increase in the amount of burned biomass across southeast Australia compared to the deglacial period, indicating a warmer and wetter climate that promoted greater vegetation growth (Mooney *et al.*, 2011).

After 6 ka, climate reconstructions from other sites in Australia (e.g., Shulmeister and Lees, 1995; Reeves *et al*., 2013; Woodward *et al*., 2014) report short-term climatic variability superimposed on a longer-term drying trend. Reconstructions of lake levels at Blue Lake (South Australia, not to be confused with the Blue Lake in this study), Lake Keilambete, and Lake Gnotuk (Figure 6) report low lake levels generally responding to increases in evapotranspiration through much of the late Holocene (Gouramanis *et al.*, 2010; Wilkins *et al.*, 2013). There is also a decrease in fire frequency across Australia beginning at around 6 ka (Mooney *et al*., 2011).

Some proxy data from the Blue Lake core might echo this; for example, LOI both peaks at about 5 cal ky BP and slightly decreases until the present experiences several shifts on the order of ~5% after ca. 8 cal ky BP (Figure 12). Log(Rb/Sr) shows an increasing trend after about 5 cal ky BP as well, which suggests that weathering rates slightly decreased in the late Holocene (Figure 13). A similar but less pronounced trend is evident in the K/Ti record of chemical weathering (Figure 13), which could also suggest decreased precipitation. These trends agree with drying during the late Holocene but could also be explained by changes in temperature or perhaps changes within the catchment's ecology that occurred independently from climate. Evidence from these proxies alone is not strong enough to confirm drying, particularly when magnetic susceptibility and grain size proxies remain stable (Figure 12).

Other records have also proposed that the Inter-tropical Convergence Zone migrated northwards during the late Holocene, which caused Australia's climate to be more strongly influenced by the El Niño-Southern Oscillation, which is characterized by decadal-scale variability (Shulmeister and Lees, 1995: Reeves *et al.*, 2013; Striewski *et al.*, 2013). While there is variability in most proxies in this record (Figures 12, 13), the shifts do not appear to be more substantial in the late Holocene than in early portions of unit 12. This does not disprove the influence of the El Niño-Southern Oscillation on the climate of the Snowy Mountains, but perhaps suggests that its effects on the environment locally were muted.

5.4.5.1 Possible evidence for the 8.2 ka event

Unit 12b (400 – 408 cm depth) is a brief interval marked by a coherent shift in several proxies, including a decrease in LOI, an increase in magnetic susceptibility, an increase in the overall fraction of sand, and an increase in log(Rb/Sr) (decreased weathering) (Figures 12, 13).

Together, these changes suggest a short-lived reduction in vegetation cover within the catchment combined with higher energy surface-water flow that allowed coarser sediments to be transported to the lake, perhaps corresponding to a cooler and/or drier climate. The mean depth-model ages of the upper and lower bounds of this unit place the timing at 8.4 – 8.2 cal ky BP, which corresponds closely to the global 8.2 ka event, but the 95% confidence interval in the age model indicates that the event could have occurred either before (9.2 – 9.0 cal ky BP) or after (7.9 – 7.5 cal ky BP) the 8.2 ka event. Global analyses of climate records spanning the 8.2 ka event suggest that the cool dry conditions observed in the North Atlantic coincided with regionally constrained warm and wet conditions in parts of the Southern Hemisphere (Morrill *et al*., 2013). However, select studies from the Southern Hemisphere have noted horizons possibly suggesting cool and/or dry conditions coincident with the 8.2 ka event, such as Fletcher *et al*. (2015) in Tasmania, Augustinus *et al.* (2008) in New Zealand, and Duan *et al.* (2021) in Madagascar, although they also document a shift towards wetter conditions. Apart from these records, evidence of the 8.2 ka event in the Trans-Australian region is sparse. At Blue Lake, a refined age-depth model and analyses of various biomarker proxies (e.g., chironomids) may help resolve whether unit 12b does indeed record a local response to the 8.2 event.

5.4.6 Late Holocene (2.2 cal ky BP – present)

While the environment surrounding Blue Lake appears to have been relatively stable during the Holocene, several proxies show minor but relatively consistent changes in unit 12d (2.2 – 1.2 cal ky BP). There is an increase in magnetic susceptibility, a decrease in LOI, and an increase in both log(Rb/Sr) and Si/Ti suggesting slightly decreased vegetation cover and

weathering in the basin (Figures 12, 13). The grain size proxies all remain relatively unchanged through this interval (Figures 12, 13).

The Little Ice Age (ca. 14th to 19th centuries) is the largest cooling event during the latest Holocene, but was probably not globally coherent (Neukom *et al*., 2019). The Little Ice Age has been recognized in Tasmania but not mainland Australia (Saunders *et al*., 2013). at Blue Lake, however, the 95% confidence interval for unit 12d varies from 2.6 – 1.8 cal ky BP to 1.4 – 1.0 cal ky BP, both earlier than published dates for the LIA (e.g., Mann *et al*., 2009).

This interval is perhaps the most notable instance of a millennial-scale environmental change at Blue Lake during the late Holocene. Shifts potentially similar to this one have been observed at a myriad of sites around Australia (e.g., Beck *et al*., 2017). A brGDGT temperature record from nearby Club Lake suggests a 2^{o} C increase in temperature between 1.6 and 1.0 cal ky BP (Thomas *et al*., 2022). Thomas *et al*. (2022) found that this increase in temperature was linked with an increase in fire activity, which was also observed from 1.6 to 1.3 ka at a nearby fen by Mooney *et al*. (1997). Although I did not analyze charcoal in this study, an increase in fire frequency could contribute to a slight decrease in vegetation and increase in clastic sediment mobilization to the lake.

After 1.2 cal ky BP, the proxies indicate a return to slightly warmer and/or wetter conditions similar to much of the earlier parts of the Holocene (Figures 12, 13). Stanley and De Deckker (2002) analyzed aeolian sediments at Blue Lake and found evidence for increased storminess during the last 1.6 ka. In this study, I did not focus on reconstructing human activity, but Mooney *et al*. (1997) note increased sedimentation rates at a nearby site resulting from grazing. The age of the uppermost sediments in the core are also unknown. The Livingstone coring system can potentially lose the uppermost sediments. Future work at this site should

emphasize obtaining and analyzing a short core of the youngest sediments to determine the impact of anthropogenic land use in the Snowy Mountains.

5.5 The Blue Lake record in a Southern Hemisphere context

The Blue Lake record has implications for the local climatic and environmental history of the Snowy Mountains but also broadly for the Southern Hemisphere. Blue Lake is situated in a region that has an unclear climate history in the context of the Bipolar Seesaw (e.g., De Deckker *et al*., 2012; Pedro *et al*., 2016). The two hemispheres experienced synchronous but opposite climate anomalies throughout portions of the deglacial and early Holocene periods, with the transition point lying somewhere near the southern mid-latitudes (De Deckker *et al*., 2012). Based on the strong ACR signal and potential lack of apparent Younger Dryas signal, the climate of Blue Lake and southeast Australia appears to align more closely with that of the high southern latitudes. During the Holocene, synoptic relationships with the rest of the Southern Hemisphere are somewhat less clear. The Blue Lake record shows evidence of a possible 8.2 ka event signal, which if validated by subsequent analyses would be unusual in the Southern Hemisphere. Additionally, the Blue Lake core has limited evidence for a climate dominated by the El Niño-Southern Oscillation as has been proposed by many Australian and Southern Hemisphere records, although this inference may relate to a limitation in the chronologic resolution in the core. Through the late Holocene (after 6 ka), there is evidence for decreased moisture availability at Blue Lake as has been observed elsewhere in Australia. However, this record does not include quantitative measures of past precipitation in the region (e.g., lake salinity), which would be needed to confirm the presence of a drying trend. Finally, there is limited evidence for the Little Ice Age at Blue Lake, which has generally not been observed in Australia with one exception

(Saunders *et al*., 2013). The Blue Lake record serves as a useful addition to the climatic and environmental history of the Southern Hemisphere; further analysis of this core and future cores planned for the other lakes in KNP should test and refine the interpretations I have presented here related to paleoclimate events that have affected the region since the LGM.

6. Conclusion

In this study, I present new constraints of maximum glacial extents and equilibrium line altitude estimates in the highest parts of the Snowy Mountains during the last glacial maximum along with a multi-proxy record of deglacial and Holocene climate change from a sediment core from Blue Lake. The maximum glacial extents I map are similar to, but slightly larger than those proposed by Barrows *et al*. (2001), and the average equilibrium line altitude in the area was approximately 1970 m (Table 1, Table 2). The Blue Lake sediment core reveals substantial environmental change in the area since deglaciation, largely reflecting shifts in climate. The age-depth model for core ABL16-LI has considerable uncertainty resulting from an unequal sample distribution and the use of bulk sediment ^{14}C samples, and therefore the exact timing and duration of fluctuations in the core are not fully resolved. The Snowy Mountains experienced several major climate reversals during the early deglacial period (18.2 – 14.9 cal ky BP) and were affected by the Antarctic Cold Reversal (14.9 – 12.6 cal ky BP). The Younger Dryas period (12.6 – 10.8 cal ky BP) appears to be relatively warm and wet. There is possible evidence for a cooling period between 10.8 – 9.7 cal ky BP. Cooling has not yet been identified in other records in Australia or elsewhere in the Southern Hemisphere and this interval may therefore represent a local depositional event. The timing of this interval remains relatively unclear because it is not close to radiocarbon samples and therefore has large age uncertainties that slightly overlap with

the Younger Dryas. The Holocene appears to have been generally warm and wet. There is preliminary evidence for slight cooling and/or drying coincident with the 8.2 ka event. There is also preliminary evidence for gradual drying after 6 cal ky BP, which has also been observed in other Australian records. Finally, all proxies react to a shift between ca. 2.2 – 1.2 cal ky BP, which could be a response to changes in climate and/or local fire regimes. The climate history interpreted from the Blue Lake record correlates more strongly with the high southern latitudes than the tropics or northern latitudes during the deglacial period. It is less clear how Blue Lake correlates with the rest of the Southern Hemisphere during the Holocene because climate appears to have been mostly relatively stable. The glacial lakes in the Snowy Mountains are excellent candidates for future climatic and environmental reconstructions. My study will provide a valuable sedimentologic foundation and a preliminary framework for such studies, which will ideally include quantitative reconstructions of temperature and precipitation from the deglacial period through the present; such records are presently lacking and will contribute to our understanding of past and future climatic and environmental change in Australia and the Southern Hemisphere.

7. References

Allen, P.A., 2008, From landscapes into geological history: Nature, v. 451, p. 274–276, doi:10.1038/nature06586.

Andres, M.S., Bernasconi, S.M., McKenzie, J.A., and Röhl, U., 2003, Southern Ocean deglacial record supports global Younger Dryas: Earth and Planetary Science Letters, v. 216, p. 515–524, doi:10.1016/S0012-821X(03)00556-9.

Augustinus, P., Bleakley, N., Deng, Y., Shane, P., and Cochran, U., 2008, Rapid change in early Holocene environments inferred from Lake Pupuke, Auckland City, New Zealand: Journal of Quaternary Science, v.23, p. 435–447, doi:10.1002/jqs.1153.

Australian Alps National Parks, 2013, Grazing:https://theaustralianalpsnationalparks.org/the-alps-partnership/culture-and-history/grazing/ (accessed December 2021).

Australian Bureau of Meteorology, 2016, What is La Niña and how does it impact Australia?**:** http://www.bom.gov.au/climate/updates/articles/a020.shtml **(**accessed May 2021).

Australian Bureau of Meteorology, 2014, What is El Niño and what might it mean for Australia?: http://www.bom.gov.au/climate/updates/articles/a008-el-nino-and-australia.shtml (accessed May 2021).

Australian Bureau of Meteorology, 2013, Indian Ocean influences on Australian climate: http://www.bom.gov.au/climate/iod/ (accessed January 2022).

Arnaud, F., Révillon, S., Debret, M., Revel, M., Chapron, E., Jacob, J., Giguet-Covex, C., Poulenard, J., and Magny, M., 2012, Lake Bourget regional erosion patterns reconstruction reveals Holocene NW European Alps soil evolution and paleohydrology, Quaternary Science Reviews, v. 51, p. 81–92, doi:10.1016/j.quascirev.2012.07.025.

Balmaks, A.V., 1984, A baseline limnology of two glacial lakes in the Kosciusko alpine region of Australia: [Honors thesis]: Canberra, Royal Military College Duntroon, University N.S.W., 240 p.

Barrows, T.T., Hope, G.S., Prentice, M.L., Fitfield, L.K., and Tims, S.G., 2011, Late Pleistocene glaciation of the Mt Giluwe volcano, Papua New Guinea: Quaternary Science Reviews, v. 30., p. 2676–2689, doi:10.1016/j.quascirev.2011.05.022.

Barrows, T.T., Lehman, S.J., Fifield, L.K., and De Deckker, P., 2007, Absence of Cooling in New Zealand and the Adjacent Ocean During the Younger Dryas Chronozone: Science, v. 318, p. 86–89, doi:10.1126/science.1145873.

Barrows, T.T., and Juggins, S.J., 2005, Sea-surface temperatures around the Australian margin and Indian Ocean during the Last Glacial Maximum: Quaternary Science Reviews, v. 24, p. 1017–1047, doi:10.1016/j.quascirev.2004.07.020.

Barrows, T.T., Stone, J.O., Fifield, L.K., and Cresswell, R.G., 2002, The timing of the Last Glacial Maximum in Australia: Quaternary Science Reviews, v. 21, p. 159–173, doi:10.-1016/S0277-3791(01)00109-3.

Barrows, T.T., Stone, J.O., Fifield, L.K, and Cresswell, R.G., 2001, Late Pleistocene Glaciation of the Kosciuszko Massif, Snowy Mountains, Australia: Quaternary Research, v. 55, p. 179–189, doi:10.1006/qres.2001.2216.

Bastian, L., Revel, M., Bayon, G., Dufour, A., and Vigier, N., 2017, Abrupt response of chemical weathering to Late Quaternary hydroclimate changes in northeast Africa: Scientific Reports, v. 6, 44231, doi:10.1038/srep44231.

Beck, K.K., Fletcher, M.-S., Gadd, P.S., Heijnis, H., and Jacobsen, G.E., 2017, An early onset of ENSO influence in the extra-tropics of the southwest Pacific inferred from a 14, 600 year high resolution multi-proxy record from Paddy's Lake, northwest Tasmania: Quaternary Science Reviews, v. 157, p. 164–175, doi:10.1016/j.quascirev.2016.12.001.

Beer, R., Heiri, O., and Tinner, W., 2007, Vegetation history, fire history and lake development recorded for 6300 years by pollen, charcoal, loss on ignition and chironomids at a small lake in southern Kyrgyzstan (Alay Range, Central Asia): The Holocene, v. 17, p. 977–985, doi: 10.1177/0959683607082413.

Blaauw, M., and Christen, J.A., 2011, Flexible paleoclimate age-depth models using an autoregressive gamma process: Bayesian Analysis, v. 6, p. 457–474, doi:10.1214/11-BA618.

Bowerman, N.D., and Clark, D.H., 2011, Holocene glaciation of the central Sierra Nevada, California: Quaternary Science Reviews, v. 30, p. 1067–1085, doi:10.1016/j.quascirev.2010.10.014.

Brady, P.V., and Carroll, S.A., 1994, Direct effects of CO_2 and temperature on silicate weathering: Possible implications for climate control: Geochimica et Cosmochimica Acta, v. 58, no. 7, p. 1853–1856, doi:10.1016/0016-7037(94)90543-6.

Burgess, J., Gillieson, D., and Spate, A., 1988, On the thermal stratification of freshwater lakes in the Snowy Mountains, Australia, and the Larsemann Hills, Antarctica: Search, v. 19, p. 147–149.

Calvo, E., Pelejero, C., De Deckker, P., and Logan, G.A., 2007, Antarctic deglacial pattern in a 30 kyr record of sea surface temperature offshore South Australia: Geophysical Research Letters, v. 34, L13707, doi:10.1029/2007GL029937.

Campbell, C., 1998, Late Holocene lake sedimentology and climate change in southern Albera, Canada: Quaternary Research, v. 49, p. 96–101, doi:10.1006/qres.1997.1946.

Cardille, J., Coe, M.T., and Vano, J.A., 2004, Impacts of Climate Variation and Catchment Area on Water Balance and Lake Hydrologic Type in Groundwater-Dominated Systems: A Generic Lake Model: Earth Interactions, v. 8, p. 1–22, doi:10.1175/10873562(2004)8<1:IOCVAC>2.0.CO;2.

Chang, J.C., Shulmeister, J., Woodward, C., Steinberger, L., Tibby, J., and Barr, C., 2015, A chironomid-inferred summer temperature reconstruction from subtropical Australia during the last glacial maximum (LGM) and the last deglaciation: Quaternary Science Reviews, v. 122, p. 282–292, doi:10.1016/j.quascirev.2015.06.006.

Clark, P.U., Dyke, A.S., Shakun, J.D., Carlson, A.E., Clark, J., Wohlfarth, B., Mitrovica, J.X., Hostetler, S.W., and McCabe, A.M., 2009, The Last Glacial Maximum: Science, v. 325, p. 710–714, doi:10.1126/science.1172873.

Colhoun, E.A., and Barrows, T.T., 2011, The Glaciation of Australia: Developments in Quaternary Science, v. 15, p. 1037–1045, doi:10.1016/B978-0-444-53447-7.00074-X.

Cuven, S., Francus, P., and Lamoureux, S., 2011, Mid to Late Holocene hydroclimatic and geochemical records from the varved sediments of East Lake, Cape Bounty, Canadian High

Arctic, Quaternary Science Reviews, v. 30, p. 2651–2665, doi:10.1016/j.quascirev.2011.05.019.

Davies, S.J., Lamb, H.F., and Roberts, S.J., 2015, Micro-XRF core scanning in paleolimnology: recent developments, *in* Croudace, I.W., and Rothwell, R.G., eds., Micro-XRF Studies of Sediment Cores, Developments in Paleoenvironmental Research, v. 17, Dordrecht, Springer, p. 189–226, doi:10.1007/978-94-017-9849-5_7.

Dean, W.E., 1974, Determination of carbonate and organic matter in calcareous sediments and sedimentary rocks by loss on ignition: Comparison with other methods: Journal of Sedimentary Petrology, v. 44, no. 1, p. 242–248, doi:10.1306/74D729D2-2B21-11D7-8648000102C1865D.

De Deckker, P., Moros, M., Perner, K., and Jansen, E., 2012, Influence of the tropics and southern westerlies on glacial interhemispheric asymmetry: Nature Geoscience, v. 5, p. 266–269, doi:10.1038/ngeo1431.

De Deckker, P., Magee, J.W., and Shelley, J.M.G., 2011, Late Quaternary palaeohydrological changes in the large playa Lake Frome in central Australia, recorded from the Mg/Ca and Sr/Ca in ostracod valves and biotic remains: Journal of Arid Environments, v. 75, p. 38–50, doi:10.1016/j.jaridenv.2010.08.004.

Doughty, A.M., Kaplan, M.R., Peltier, C., and Barker, S., 2021, A maximum in global glacier extent during MIS 4: Quaternary Science Reviews, v. 261, 106948, doi:10.1016/j.quascirev.2021.106948.

Douglass, D.C., Singer, B.S., Kaplan, M.R., Mickelson, D.M., and Caffee, M.W., 2006, Cosmogenic nuclide surface exposure dating of boulders on last-glacial and late-glacial moraines, Lago Buenos Aires, Argentina: Interpretive strategies and paleoclimate implications: Quaternary Geochronology, v. 1, no. 1., p. 43–58, doi:10.1016/j.quageo.2006.06.001.

Duan, P., Li, H., Sinha, A., Voarintsoa, N.R.G., Kathayat, G., Hu, P., Zhang, H., Ning, Y., and Cheng, H., 2021, The timing and structure of the 8.2 ka event revealed through high-resolution speleothem records from northwestern Madagascar: Quaternary Science Review, v. 268, 107104, doi:10.1016/j.quascirev.2021.107104.

Ellerton, D., Shulmeister, J., Woodward, C., and Moss, P., 2017, Last Glacial Maximum and Last Glacial-Interglacial Transition pollen record from northern NSW, Australia: evidence for a humid late Last Glacial Maximum and dry deglaciation in parts of eastern Australia: Journal of Quaternary Science, v. 32, p. 717–728, doi:10.1002/jqs.2960.

Fernández, M., Björck, S., Wohlfarth, B., Maidana, N.I., Unkel, I., and Van der Putten, N., 2013, Diatom assemblage changes in lacustrine sediments from Isla de los Estados, southernmost South America, in response to shifts in the southwesterly wind belt during the last deglaciation: Journal of Paleolimnology, v. 50, p. 433–446, doi:10.1007/s10933-013-9736-4.

Fitzsimmons, K.E. *et al.*, 2013, Late Quaternary palaeoenvironmental change in the Australian drylands: Quaternary Science Reviews, v. 74, p. 78–96, doi:10.1016/j.quascirev.2012.09.007.

Fletcher, M.-S., *et al*., 2021, Northward shift of the southern westerlies during the Antarctic Cold Reversal: Quaternary Science Reviews, v. 271, 107189, doi:10.1016/j.quascirev.2021.107189.

Fletcher, M.-S., Benson, A., Heijnis, H., Gadd, P.S., Cwynar, L.C., Rees, A.B.H., 2015, Changes in biomass burning mark the onset of an ENSO-influenced climate regime at 42°S in southwest Tasmania, Australia: Quaternary Science Reviews, v. 122, p. 222–232, doi:10.1-016/j.quascirev.2015.05.002.

Foster, I.D.L., Albon, A.J., Bardell, K.M., Fletcher, J.L., Jardine, T.C., Mothers, R.J., Pritchard, M.A., and Turner, S.E., 1991, High energy coastal sedimentary deposits; and evaluation of depositional processes in Southwest England: Earth Surface Processes and Landforms, v. 16, no. 4, p. 341–356, doi:10.1002/esp.3290160407.

Gallant, J., Wilson, N., Dowling, T., Read, A., and Inskeep, C., 2011, SRTM-derived Digital Elevation Models Version 1.0: Geoscience Australia, https://ecat.ga.gov.au/geonetwork-/srv/eng/catalog.search#/metadata/72759.

Galloway, R.W., 1965, Late Quaternary Climates in Australia: The Journal of Geology, v. 73, no. 4, p. 603–618.

García-Ruiz, J.M., Palacios, D., González-Sampériz, P., de Andrés, N., Moreno, A., Valero-Garcés, B., and Gómez-Villar, A., 2016, Mountain glacier evolution in the Iberian Peninsula during the Younger Dryas: Quaternary Science Reviews, v. 138, p. 16–30, doi:10.1016/j.qu-ascirev.2016.02.022.

Gillespie, A.R., and Clark, D.H., 2011, Glaciations of the Sierra Nevada, California, USA: Developments in Quaternary Science, v. 15, p. 447–462, doi:10.1016/B978-0-444-53447-7.00034-9.

Glasser, N. F., Harrison, S., Schnabel, C., Fabel, D., and Jansson, K.N., 2012, Younger Dryas and early Holocene age glacier advances in Patagonia: Quaternary Science Reviews, v. 58, p. 7–17, doi:10.1016/j.quascirev.2012.10.011.

Graham, A.G.C., *et al*., 2017, Major advance of South Georgia glaciers during the Antarctic Cold Reversal following extensive sub-Antarctic glaciation: Nature Communications, v. 8, 14798, doi:10.1038/ncomms14798.

Grimm, E.C., Maher Jr., L.J., and Nelson, D.M., 2009, The magnitude of error in conventional bulk-sediment radiocarbon dates from central North America: Quaternary Research, v. 72, p. 301 – 308, doi:10.1016/j.yqres.2009.05.006.

Goede, A., McDermott, F., Hawkesworth, C., Webb, J., and Finlayson, B., 1996, Evidence of Younger Dryas and Neoglacial cooling in a Late Quaternary palaeotemperature record from a speleothem in eastern Victoria, Australia: Journal of Quaternary Science, v. 11, p. 17, doi:10.1002/(SICI)1099-1417(199601/02)11:1<1::AID-JQS219>3.0.CO;2-2.

Gong, D., and Wang, S., 1999, Definition of Antarctic oscillation index, 1999, Geophysical Research Letters, v. 206, no. 4, p. 459–462, doi:10.1029/1999GL900003.

Gouramanis, C., De Deckker, P., Switzer, A.D., and Wilkins, D., 2013, Cross-continent comparison of high-resolution Holocene climate records from southern Australia – Deciphering the impacts of far-field teleconnections: Earth Science Reviews, v. 121, p. 55–72, doi:10.1016/j.earscirev.2013.02.006.

Gouramanis, C., Wilkins, D., and De Deckker, P., 2010, 6000 years of environmental changes recorded in Blue Lake, South Australia, based on ostracod ecology and valve chemistry: Palaeogeography, Palaeoclimatology, Palaeoecology, v. 297, p. 223–237, doi:10.1016-/j.palaeo.2010.08.005.

Haberle, S.G., 2005, A 23,000-yr Pollen Record from Lake Euramoo, Wet Tropics of NE Queensland, Australia: Quaternary International, v. 64, p. 343–356, doi:10.1016/j.yqres.20-05.08.013.

Harrison, S.P., and Metcalfe, S.E., 1985, Variations in Lake Levels during the Holocene in North America: An Indicator of Changes in Atmospheric Circulation Patterns: Géographie physique et Quaternaire, v. 39, no. 2, p. 141–150, doi:10.7202/032598ar.

Heiri, O., Lotter, A.F., and Lemcke, G., 2001, Loss on ignition as a method for estimating organic and carbonate content in sediments: reproducibility and comparability of results: Journal of Paleolimnology, v. 25, p. 101–110, doi:10.1023/A:1008119611481.

Hendon, H.H., Thompson, D.W.J., and Wheeler, M.C., 2007, Australian rainfall and surface temperature variations associated with the Southern Hemisphere Annular Mode: Journal of Climate, v. 20, p. 2452–2467, doi:10.1175/JCLI4134.1.

Heymann, C., Nelle, O., Dörfler, W., Zagana, H., Nowaczyk, N., Xue, J., and Unkel, I., 2013, Late Glacial to mid-Holocene palaeoclimate development of Southern Greece inferred from the sediment sequence of Lake Stymphalia (NE-Peloponnese): Quaternary International, v. 302, p. 42–60, doi:10.1016/j.quaint.2013.02.014.

Hinojosa, J.L., Moy, C.M., Vandergoes, M., Feakins, S.J., and Sessions, A.L., 2019, Hydrologic Change in New Zealand During the Last Deglaciation Linked to Reorganization of the Southern Hemisphere Westerly Winds: Paleoceanography and Paleoclimatology, v. 34, p. 2158–2170, doi:10.1029/2019PA003656.

Hogg, A.G., *et al*., 2020, SHCal20 Southern Hemisphere Calibration, 0–55,000 Years cal BP: Radiocarbon, v. 62, p. 759–778, doi:10.1017/RDC.2020.59.

Hope, G., 2009, Environmental change and fire in the Owen Stanley Ranges, Papua New Guinea: Quaternary Science Reviews, v. 28, p. 2261–2276, doi:10.1016/j.quascirev-.2009.04.012.

Howarth, J.D., *et al*., 2021, Calibrating the marine turbidite paleaeoseismometer using the 2016 Kaikōura earthquake: Nature Geoscience, v. 14, p. 161–167, doi:10.1038/s41561-021-00692-6.

Jiang, N., and Yan, Q., 2020, Evolution of the meridional shift of the subtropical and subpolar westerly jet over the Southern Hemisphere during the past 21,000 years: Quaternary Science Reviews, v. 246, 106544, doi:10.1016/j.quascirev.2020.106544.

Jin, Z., Cao, J., Wu, J., and Wang, S., 2006, A Rb/Sr record of catchment weathering response to Holocene climate change in Inner Mongolia: Earth Surface Processes and Landforms, v. 31, p. 285–291, doi:10.1002/esp.1243.

Kaplan, M.R., Schaefer, J.M., Denton, G.H., Barrell, D.J.A., Chinn, T.J.H., Putnam, A.E., Andersen, B.G., Finkel, R.C., Schwartz, R., and Doughty, A.M., 2010, Glacier retreat in New Zealand during the Younger Dryas stadial: Nature, v. 467, p. 194–197, doi:10.1038-/nature09313.

Kaplan, M.R., Akert, Jr., R.P., Singer, B.S., Douglass, D.C., and Kurz, M.D., 2004, Cosmogenic nuclide chronology of millennial-scale glacial advances during O-isotope stage 2 in Patagonia: GSA Bulletin, v. 116, no. 3/4, p. 308–321, doi:10.1130/B25178.1.

Kershaw, A.P., McKenzie, G.M., Porch, N., Roberts, R.G., Brown, J., Heijnis, H., Orr, M.L., Jacobsen, G., and Newall, P.R., 2007, A high-resolution record of vegetation and climate through the last glacial cycle from Caledonia Fen, southeastern highlands of Australia: Journal of Quaternary Science, v. 22, p. 481–500, doi:10.1002/jqs.1127.

Kobashi, T., Severinghaus, J.P., Brook, E.J., Barnola, J.-M., and Grachev, A.M., 2007, Precise timing and characterization of abrupt climate change 8200 years ago from air trapped in polar ice: Quaternary Science Reviews, v. 26, p. 1212–1222, doi:10.1016/j.quascirev.2007-.01.009.

Kolbe, P., and Taylor, S.R., 1966, Geochemical investigation of the granitic rocks of the snowy mountains area, New South Wales: Journal of the Geological Society of Australia, v. 13, no. 1, p. 1–25, doi:10.1080/00167616608728603.

Kylander, M.E., Klaminder, J., Wohlfarth, B., and Löwemark, L., 2013, Geochemical responses to paleoclimatic changes in southern Sweden since the late glacial: the Hässeldala Port lake sediment record: Journal of Paleolimnology, v. 50, p. 57–70, doi:10.1007/s10933-013-9704-z.

Kylander, M.E., Ampel, L., Wohlfarth, B., and Veres, D., 2011, High-resolution X-ray fluorescence core scanning analysis of Les Echets (France) sedimentary sequence: new insights from chemical proxies: Journal of Quaternary Science, v. 26, p. 109–117, doi:10.1-002/jqs.1438.

Laird, K.R., Fritz, S.C., Cumming, B.F., and Grimm, E.C., 1998, Early-Holocene limnological and climatic variability in the Northern Great Plains: The Holocene, v. 8, p. 275–285, doi:10.1191/095968398673895438.

Last, W.M., 2001, Textural analysis of lake sediments, *in* Last, W.M., and Smol, J.P., eds., Tracking Environmental Change Using Lake Sediments, Volume 2: Physical and Geochemical Methods, Dordrecht, Netherlands, Kluwer Academic Publishers, p. 41–81.

Lee, S., and Kim, H.-K., 2003, The dynamical relationship between subtropical and eddy-driven jets: Journal of the Atmospheric Sciences, v. 60, p. 1490–1503, doi:10.1175/1520-0469(2003)060<1490:TDRBSA>2.0.CO;2.

Leonard, E.M., 1989, Climatic Change in the Colorado Rocky Mountains: Estimates Based on Modern Climate at Late Pleistocene Equilibrium Lines: Arctic and Alpine Research, v. 21, p. 245, doi:10.2307/1551563.

Leunda, M., González-Sampériz, P., Gil-Romera, G., Aranbarri, J., Moreno, A., Oilva-Urcia, B., Sevilla-Callejo, M., and Valero-Garcés, B., 2017, The Late-Glacial and Holocene Marboré Lake sequence (2612 m a.s.l., Central Pyrenees, Spain): Testing high altitude sites sensitivity to millennial scale vegetation and climate variability: Global and Planetary Change, v. 157, p. 214–231, doi:j.gloplacha.2017.08.008.

Livingstone, D.A., 1955, A Lightweight Piston Sampler for Lake Deposits: Ecology, v. 36, p. 137–139, doi:10.2307/1931439.

Mann, M.E., Zhang, Z., Rutherford, S., Bradley, R.S., Hughes, M.K., Shindell, D., Ammann, C., Faluvegi, G., and Ni, F., 2009, Global Signatures and Dynamical Origins of the Little Ice

Age and Medieval Climate Anomaly: Science, v. 326, p. 1256–1260, doi:10.1126/science.-1177303.
Mann, M.E., 2002, Little Ice Age, *in* MacCracken, M.C., and Perry, J.S., eds., Encyclopedia of Global Environmental Change, Volume 1, The Earth system: physical and chemical dimensions of global environmental change: Chichester, UK, John Wiley & Sons Ltd, p. 504–509.
McGee, D., Moreno-Chamarro, E., Green, B., Marshall, J., Galbraith, E., and Bradtmiller, L., 2018, Hemispherically asymmetric trade wind changes as signatures of past ITCZ shifts: Quaternary Science Reviews, v. 180, p. 214–228, doi:10.1016/j.quascirev.2017.11.020.
Mendelová, M., Hein, A.S., Rodés, Á., Smedley, R.K., and Xu, S., 2020, Glacier expansion in central Patagonia during the Antarctic Cold Reversal followed by retreat and stabilisation during the Younger Dryas: Quaternary Science Reviews, v. 227, 106047, doi:10.1016/j.quascirev.2019.106047.
Meyers, P.A., 2003, Applications of organic geochemistry to paleolimnological reconstructions: a summary of examples from the Laurentian Great Lakes: Organic Geochemistry, v. 34, p. 261–289, doi:10.1016/S0146-6380(02)00168-7.
Meyers, P.A., and Lallier-Vergès, E., 1999, Lacustrine sedimentary organic matter records of Late Quaternary paleoclimates: Journal of Paleolimnology, v. 21, p. 345–372, doi:10.1023/-A:1008073732192.
Meyers, P.A., and Ishiwatari, R., 1995, Organic Matter Accumulation Records in Lake Sediments, *in* Lerman, A., Imboden, D.M., and Gat, J. R., eds., Physics and Chemistry of Lakes: Berlin, Heidelberg, Springer, p. 279–328, doi:10.1007/978-3-642-85132-2_10.
Mooney, S.D. *et al.*, 2011, Late Quaternary fire regimes of Australasia: Quaternary Science Reviews, v. 30, p. 28–46, doi:10.1016/j.quascirev.2010.10.010.
Mooney, S.D., Watson, J.R., and Dodson, J.R., 1999: Late Holocene environmental change in an upper montane area of the Snowy Mountains, New South Wales: The Australian Geographer, v. 28, p. 185–200, doi:10.1080/00049189708703192.
Moreno, A., Giralt, S., Valero-Garcés, B., Sáez, A., Bao, R., Pueyo, J.J., González-Sampériz, P., and Taberner, C., 2007, A 14 kyr record of the tropical Andes: The Lago Chungará sequence (18°S, northern Chilean Altiplano)**,** Quaternary International, v. 161, p. 4–21, doi:10.1016/j.quaint.2006.10.020.
Morrill, C., Anderson, D.M., Bauer, B.A., Buckner, R., Gille, E.P., Gross, W.S., Hartman, M., and Shah, A., 2013, Proxy benchmarks for intercomparison of 8.2 ka simulations: Climates of the Past, v. 9, p. 423–432, doi:10.5194/cp-9-423-2013.
Nesje, A., and Dahl, S.O., 2001, The Greenland 8200 cal. yr BP event detected in loss-on-ignition profiles in Norwegian lacustrine sediment sequences: Journal of Quaternary Science, v. 16, no. 2, p. 155–166, doi:10.1002/jqs.567.
Neukom, R., Steiger, N., Gómez-Navarro, J.J., Wang, J., and Werner, J.P., 2019, No evidence for globally coherent warm and cold periods over the preindustrial Common Era: Nature, v. 571, p. 550–554, doi:10.1038/s41586-019-1401-2.
NOAA Climate Prediction Center, 2012, Frequently Asked Questions about El Niño and La Niña: https://www.cpc.ncep.noaa.gov/products/analysis_monitoring/ensostuff/ensofaq.-shtml#NEUTRAL (accessed September 2021).

Ohlendorf, C., Sturm, M., and Hausmann, S., 2003, Natural environmental changes and human impact reflected in sediments of a high alpine lake in Switzerland: Journal of Paleolimnology, v. 30, p. 297–306, doi:10.1023/A:1026032829150.

Osmaston, H., 2005, Estimates of glacier equilibrium line altitudes by the Area×Altitude, the Area×Altitude Balance Ratio and the Area×Altitude Balance Index methods and their validation: Quaternary International, v. 138–139, p. 22–31, doi:10.1016/j.quaint.2005.02.0-04.

Pedro, J.B. *et al.*, 2016, The spatial extent and dynamics of the Antarctic Cold Reversal: Nature Geoscience, v. 9, p. 51–55, doi:10.1038/ngeo2580.

Pedro, J.B., van Ommen, T.D., Rasmussen, S.O., Morgan, V.I., Chappellaz, J., Moy, A.D., Masson-Delmotte, V., and Delmotte, M., 2011, The last deglaciation: timing the bipolar seesaw: Climates of the Past Discussions, v. 7, p. 397–430, doi:10.5194/cpd-7-397-2011.

Pellitero, R., Rea, B.R., Spagnolo, M., Bakke, J., Ivy-Ochs, S., C.R., Hughes, P., Lukas, S., and Ribolini, A., 2015, A GIS tool for automatic calculation of glacier equilibrium-line altitudes: Computers & Geosciences, v. 82, p. 55–62, doi:10.1016/j.cageo.2015.05.005.

Perdue, E.M., and Koprivnjak, J-.F., 2007, Using the C/N ratio to estimate terrigenous inputs of organic matter to aquatic environments: Estuarine, Coastal, and Shelf Science, v. 73, p. 65–72, doi:10.1016/j.ecss.2006.12.021.

Petherick, L.M., Moss, P., and McGowan, H., 2017, An extended Last Glacial Maximum in subtropical Australia: Quaternary International, v. 432A, p. 1–12, doi:10.1016/j.quaint.2015.11.015.

Petherick, L.M. *et al.*, 2013, Climatic records over the past 30 ka from temperate Australia – a synthesis from the Oz-INTIMATE workgroup: Quaternary Science Reviews, v. 74, p. 58–77, doi:10.1016/j.quascirev.2012.12.012.

Petherick, L.M., McGowan, H.A., and Kamber, B.S., 2009, Reconstructing transport pathways for late Quaternary dust from eastern Australia using the composition of trace elements of long traveled dusts: Geomorphology, v. 105, p. 67–79, doi:10.1016/j.geomorph.2007.12.015.

Putnam, A.E., Denton, G.H., Schaefer, J.M., Barrell, D.J.A., Andersen, B.G., Finkel, R.C., Schwartz, R., Doughty, A.M., Kaplan, M.R., and Schlüchter, C., 2010, Glacier advance in southern middle-latitudes during the Antarctic Cold Reversal: Nature Geoscience, v. 3, p. 700–704, doi:10.1038/ngeo962.

Raine, J.I., 1982, Dimictic thermal regime and morphology of Blue Lake in the Snowy Mountains of New South Wales: Australian Journal of Marine and Freshwater Research, v. 33, no. 6, p. 1119–1122, doi:10.1071/MF9821119.

Raine, J.I., 1974, Pollen sedimentation in relation to the Quaternary vegetation history of the Snowy Mountains of New South Wales [Ph.D.]: Australian National University, 387 p.

Rasmussen, S.O., *et al*., 2006, A new Greenland ice core chronology for the last glacial termination: Journal of Geophysical Research, v. 111, D06102, doi:10.1029/2005JD006079.

Rea, B.R., 2009, Defining modern day Area-Altitude Balance Ratios (AABRs) and their use in glacier-climate reconstructions: Quaternary Science Reviews, v. 28, p. 237–248, doi:10.1016/j.quascirev.2008.10.011.

Reasoner, M.A., Osborn, G., and Rutter, N.W, 1994. Age of the Crowfoot advance in the Canadian Rocky Mountains: A glacial event coeval with the Younger Dryas oscillation: Geology, v. 22, p. 439–442, doi:10.1130/0091-7613(1994)022<0439:AOTCAI>2.3.CO;2.

Reeves, J.M., *et al.*, 2013, Climate variability over the last 35,000 years recorded in marine and terrestrial archives in the Australian region: an OZ-INTIMATE compilation: Quaternary Science Reviews, v. 74, p. 21–34, doi:10.1016/j.quascirev.2013.01.001.

Reimer, P.J., *et al.*, 2020: The IntCal20 Northern Hemisphere radiocarbon age calibration curve (0-55 cal kB): Radiocarbon, v. 62, p. 725–757, doi:10.1017/RDC.2020.41.

Sagredo, E.A., Kaplan, M.R., Araya, P.S., Lowell, T.V., Aravena, J.C., Moreno, P.I., Kelly, M.A., and Schaefer, J.M., 2018, Trans-pacific glacial response to the Antarctic Cold Reversal in the southern mid-latitudes: Quaternary Science Reviews, v. 188, p. 160–166, doi:10.1016/j.quascirev.2018.01.011.

Saji, N.H., Goswami, B.N., Vinayachandran, P.N., and Yamagata, T., 1999, A dipole mode in the tropical Indian Ocean: Nature, v. 401, p. 360–363, doi:10.1038/43854.

Sharp, K.R., 2004, Cenozoic volcanism, tectonism and stream derangement in the Snowy Mountains and northern Monaro of New South Wales: Australian Journal of Earth Sciences, v. 51, no. 1, p. 67–83, doi:10.1046/j.1400-0952.2003.01045.x.

Shulmeister, J., Thackray, G., Rittenour, T., Fink, D., and Patton, N., 2019, The timing and nature of the last glacial cycle in New Zealand: Quaternary Science Reviews, v. 206, p. 1–20, doi:10.1016/j.quascirev.2018.12.020.

Shulmeister, J., and Lees, B.G., 1995, Pollen evidence from tropical Australia for the onset of an ENSO-dominated climate at c. 4000 BP: The Holocene, v. 5, p. 10–18, doi:10.1177/095968369500500102.

Stanley, S., and De Deckker, P., 2002, A Holocene record of allochthonous, aeolian mineral grains in an Australian alpine lake; implications for the history of climate change in southeastern Australia: Journal of Paleolimnology, v. 27, p. 207–219, doi:10.1023/A:1014-249404845.

Striewski, B., Shulmeister, J., Augustinus, P.C., and Soderholm, J., 2013, Late Holocene climate variability from Lake Pupuke maar, Auckland, New Zealand: Quaternary Science Reviews, v. 77, p. 46–54, doi:10.1016/j.quascirev.2013.07.003.

Stuiver, M., Reimer, P.J., and Reimer, R.W., 2021, CALIB 8.2 [WWW program] at http://calib.org.

Tibby, J., 2012, The Younger Dryas: Relevant in the Australian region?: Quaternary International, v. 253, p. 47–54, doi:10.1016/j.quaint.2012.01.003.

Thomas, E.R., Wolff, E.W., Mulvaney, R., Steffensen, J.P., Johnsen, S.J., Arrowsmith, C., White, J.W.C., Vaughn, B., and Popp, T., 2007, The 8.2 event from Greenland ice cores: Quaternary Science Reviews, v. 26, p. 70–81, doi:10.1016/j.quascirev.2006.07.017.

Thompson, R., Kamenik, C., and Schmidt, R., 2005, Ultra-sensitive Alpine lakes and climate change: Journal of Limnology, v. 64, no. 2, p. 139–152, doi:jlimnol.2005.139.

Thomas, Z.A., *et al.*, 2022, Late Holocene climate anomaly concurrent with fire activity and ecosystem shifts in the eastern Australian Highlands: Science of The Total Environment, v. 802, 149542, doi:10.1016/j.scitotenv.2021.149542.

Thorndycraft, V.R., Bendle, J.M., Benito, G., Davies, B.J., Sancho, C., Palmer, A.P., Fabel, D., Medialdea, A., and Martin, J.R.V., 2019, Glacial lake evolution and Atlantic-Pacific drainage reversals during deglaciation of the Patagonia Ice Sheet: Quaternary Science Reviews, v. 203, p. 102–127, doi:10.1016/j.quascirev.2018.10.036.

Toggweiler, J.R., Russell, J.L., and Carson, S.R., 2006, Midlatitude westerlies, atmospheric CO_2, and climate change during the ice ages: Paleoceanography, v. 21, PA2005, doi:10.1029/2005PA001154.

Trenberth, K.E., 1997, The definition of El Niño: Bulletin of the American Meteorological Society, v. 78, no. 12, p. 2771–2777, doi:10.1175/15200477(1997)078<2771:TDOENO->2-.0.CO;2.

Walker, M., *et al*., 2018, Formal ratification of the subdivision of the Holocene Series/ Epoch (Quaternary System/Period): two new Global Boundary Stratotype Sections and Points (GSSPs) and three new stages/ subseries: Episodes, v. 41, p. 213–233, doi:10.18814/epiiugs/2018/018016.

West, A.J., Galy, A., and Bickle, M., 2005, Tectonic and climatic controls on silicate weathering: Earth and Planetary Science Letters, v. 235, p. 211–228, doi:10.1016/j.epsl.2005.03.020.

Wilkins, D., Gouramanis, C., De Deckker, P., Fifield, L.K., and Olley, J., 2013, Holocene lake-level fluctuations in Lakes Keilambete and Gnotuk, southwestern Victoria, Australia: The Holocene, v. 23, p. 784–795, doi:10.1177/0959683612471983.

Williams, M., Cook, E., van der Kaars, S., Barrows, T., Shulmeister, J., and Kershaw, P., 2009, Glacial and deglacial climatic patterns in Australia and surrounding regions from 35 000 to 10 000 years ago reconstructed from terrestrial and near-shore proxy data: Quaternary Science Reviews, v. 28, p. 2398–2419, doi:10.1016/j.quascirev.2009.04.020.

Williams, N.J., Harle, K.J., Gale, S.J., and Heijnis, H., 2006, The vegetation history of the last glacial–interglacial cycle in eastern New South Wales, Australia: Journal of Quaternary Science, v. 21, p. 735–750, doi:10.1002/jqs.1069.

Woodward, C., Shulmeister, J., Bell, D., Haworth, R., Jacobsen, G., and Zawadzki, A., 2014, A Holocene record of climate and hydrological changes from Little Llangothlin Lagoon, south eastern Australia: The Holocene, v. 24, p. 1665–1674, doi:10.1177/0959683614551218.

Wright, H. E. Jr, 1980, Cores of soft lake sediments: Boreas, v. 9, p. 107–114, doi:10.1111/j.1502-3885.1980.tb01032.x.

Wyborn, D., Owen, M., and Wyborn, L., 1990, Geology of the Kosciuszko National Park: Bureau of Mineral Resources, Canberra, scale 1:250,000.

Zolitschka, B., Francus, P., Ojala, A.E.K., and Schimmelmann, A., 2015, Varves in lake sediments – a review: Quaternary Science Reviews, v. 117, p. 1–41, doi:10.1016/j.quascirev.2015.03.019.

8. Figures

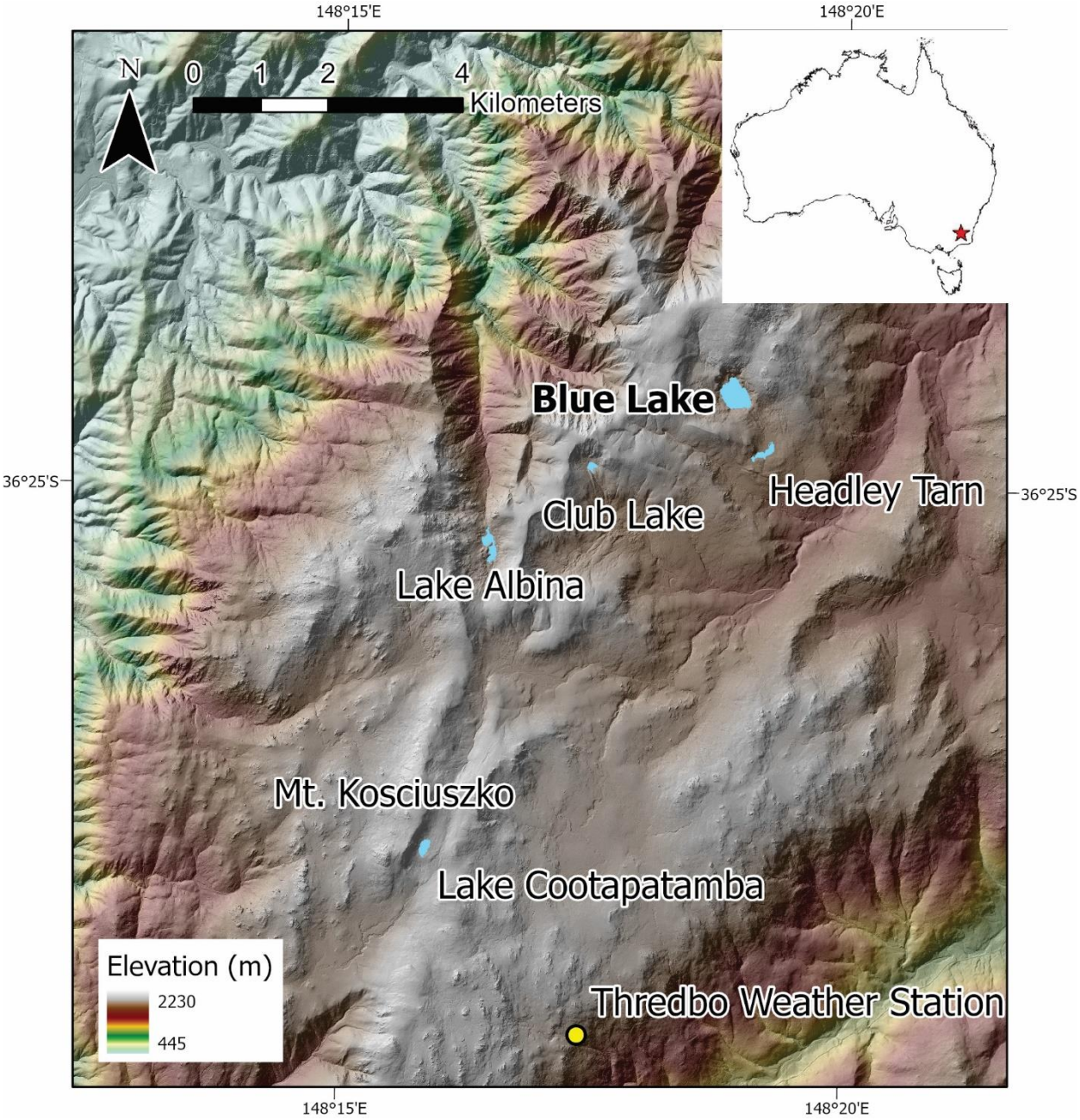

Figure 1. Lidar relief map of the highest parts of the Snowy Mountains showing the locations of Mt. Kosciuszko, the five tarns, and the Thredbo Weather Station. The location of Kosciuszko National Park is shown by the red star in the upper right corner. Lidar data from Gallant *et al*. (2011).

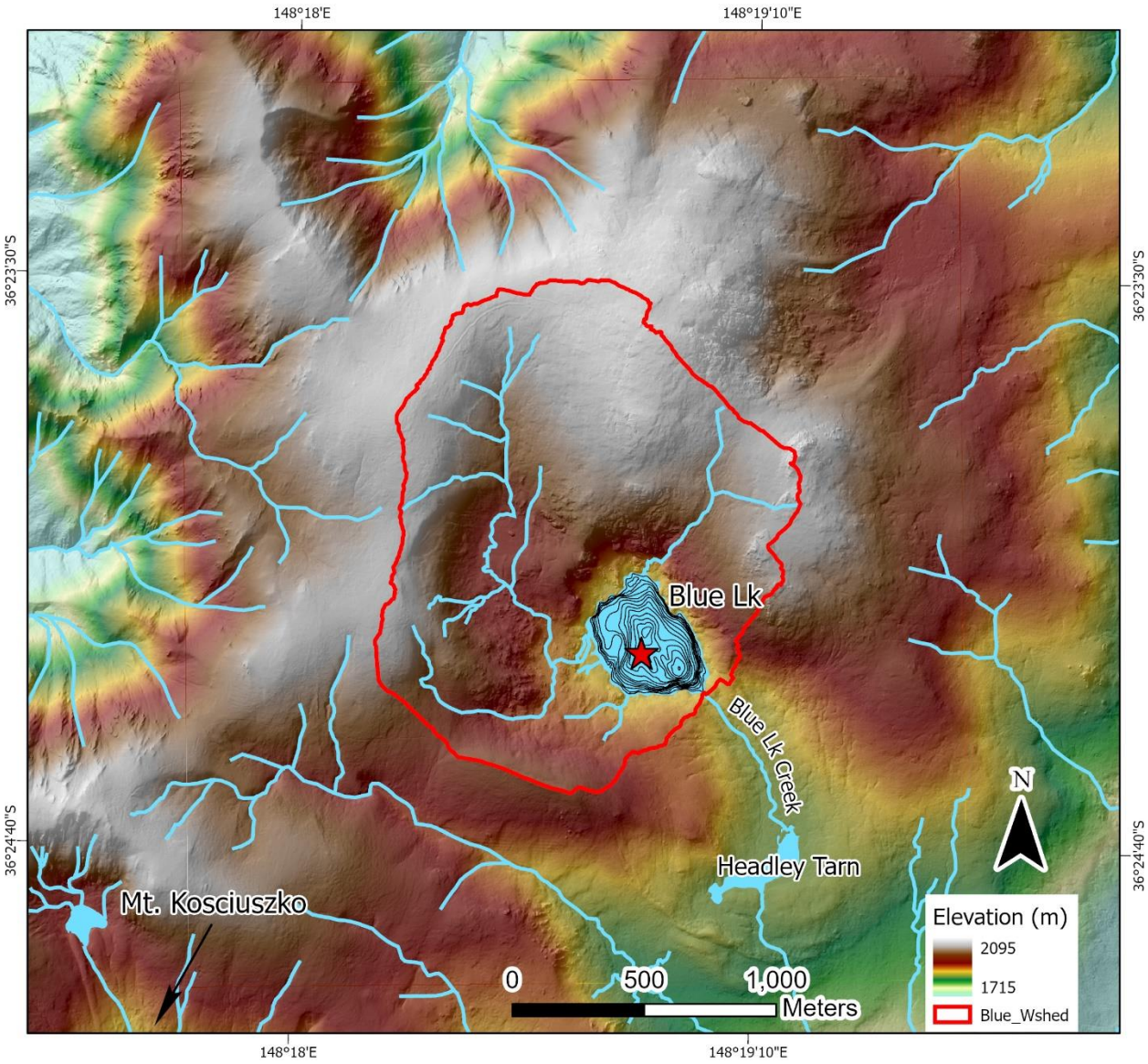

Figure 2. Lidar relief map of Blue Lake catchment (marked by the red outline) with 2-meter bathymetric contours from Dulhunty (1945); red star indicates location of core ABL16-L1. Lidar data from Gallant *et al*. (2011).

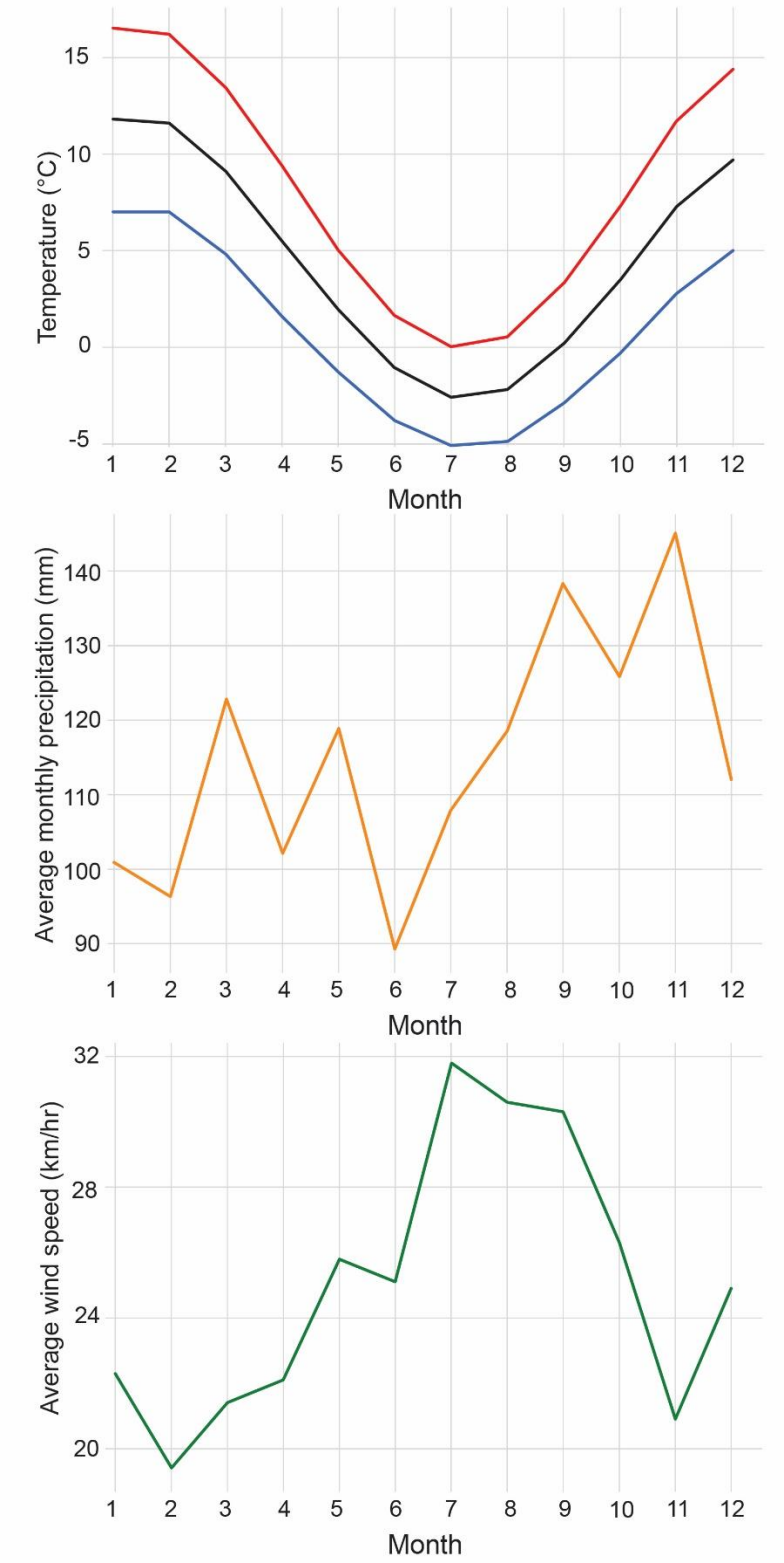

Figure 3. Modern climate data binned by month from the Thredbo weather station ~10 km south of Blue Lake (36º29'24"S, 148º17'24"E). From top to bottom: average maximum (red line) and minimum (blue line) with mean daily temperature (black line), average daily wind speed, average precipitation, average daily wind speed.

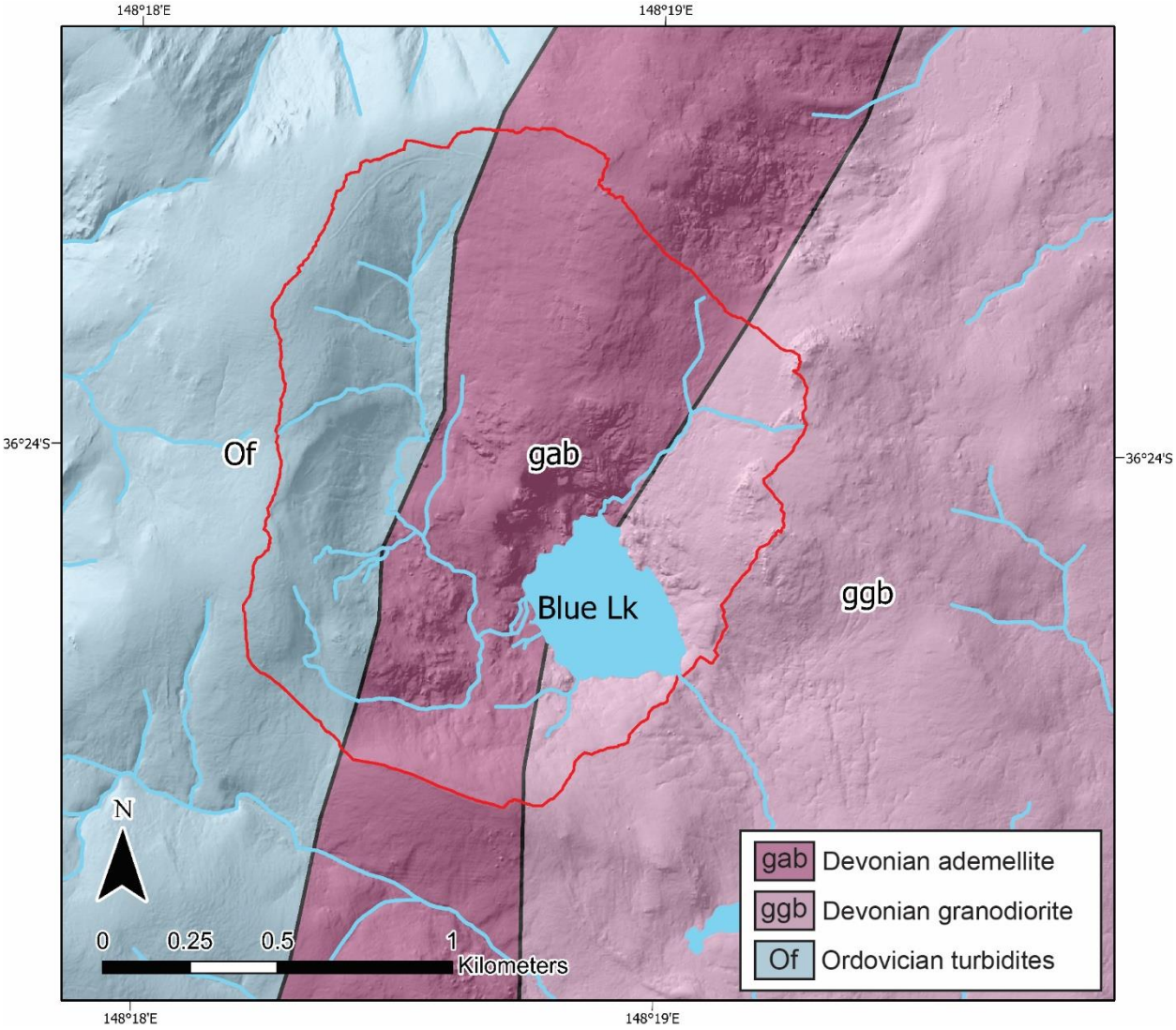

Figure 4. Geologic units in the Blue Lake catchment (red outline). Geology from Wyborn *et al*. (1990). Lidar data from Gallant *et al*. (2011).

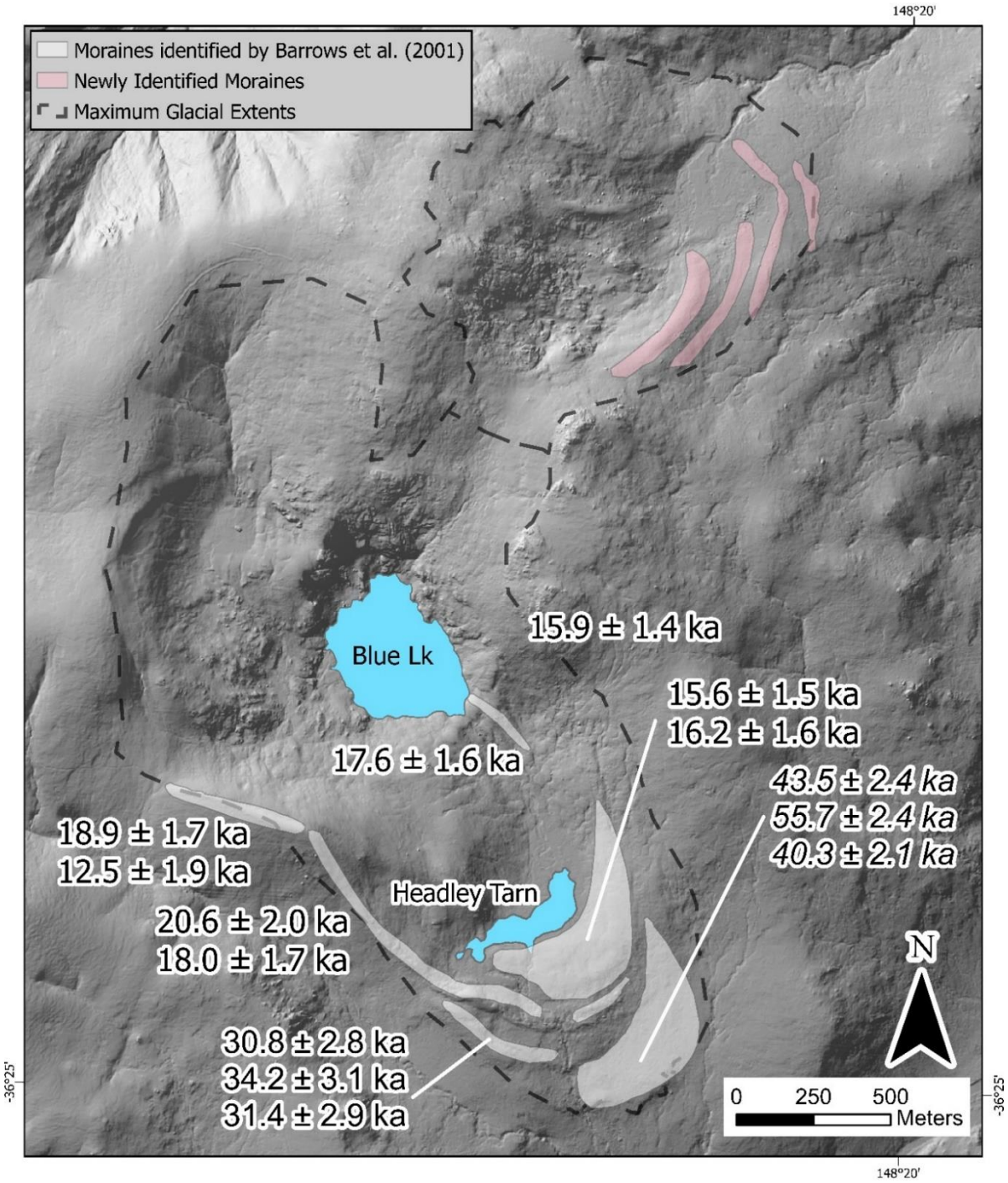

Figure 5. Moraine deposits at Blue Lake according to Barrows *et al*. (2001) superimposed on lidar hillshade. ^{10}Be cosmogenic radionuclide dates for boulders on the moraines below Blue Lake indicated (dates in standard font are from Barrows *et al.* (2001) and dates in italics are from Barrows *et al*. (2001) and were recalculated by Doughty *et al*. (2021) using the most recent production rates). Moraines colored in pink have been identified and mapped in this study based on the lidar data. Maximum inferred ice extents are outlined in dashed black lines. Lidar data from Gallant *et al*. (2011).

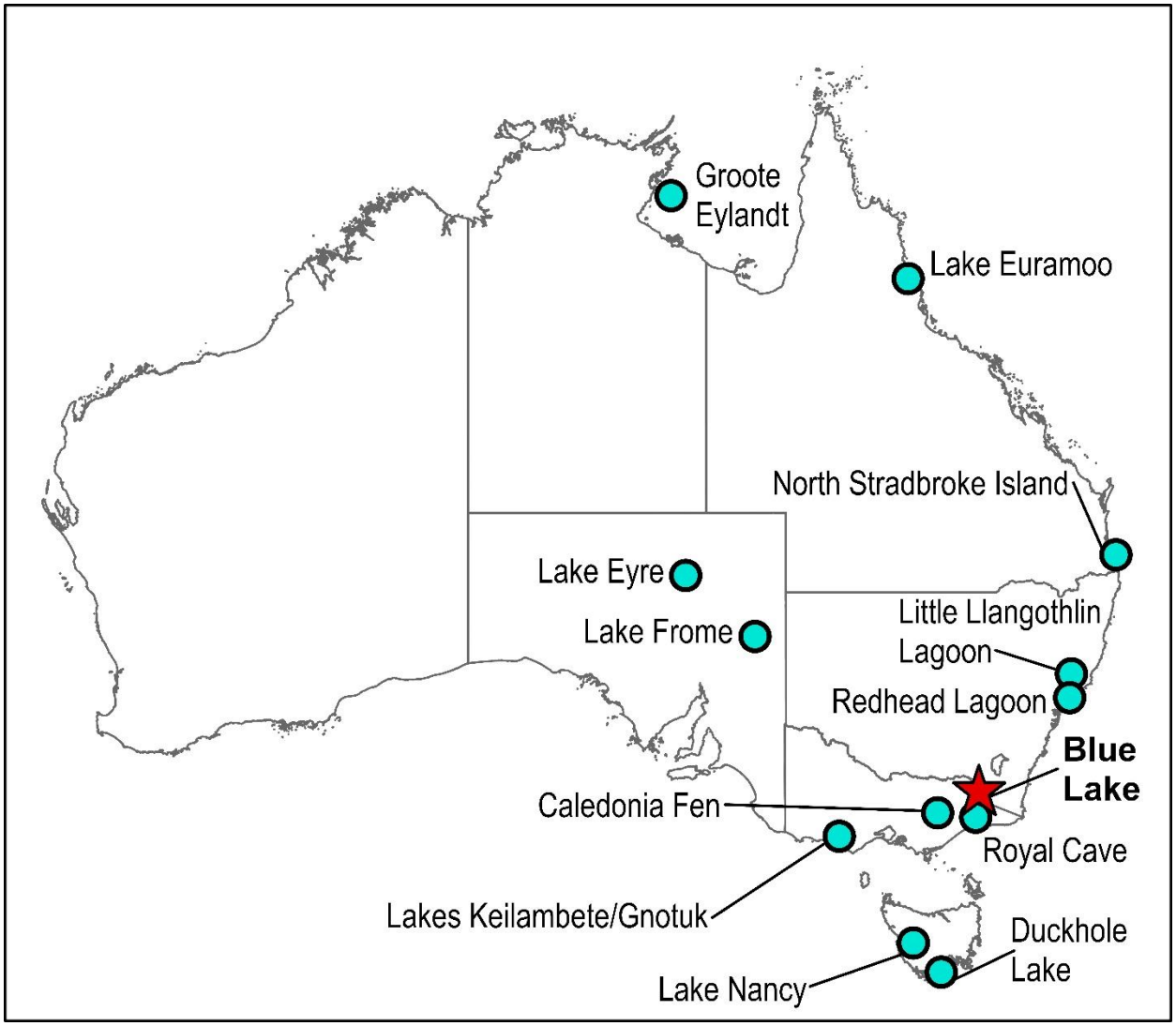

Figure 6. Locations of terrestrial paleoclimate records in Australia referred to in the text.

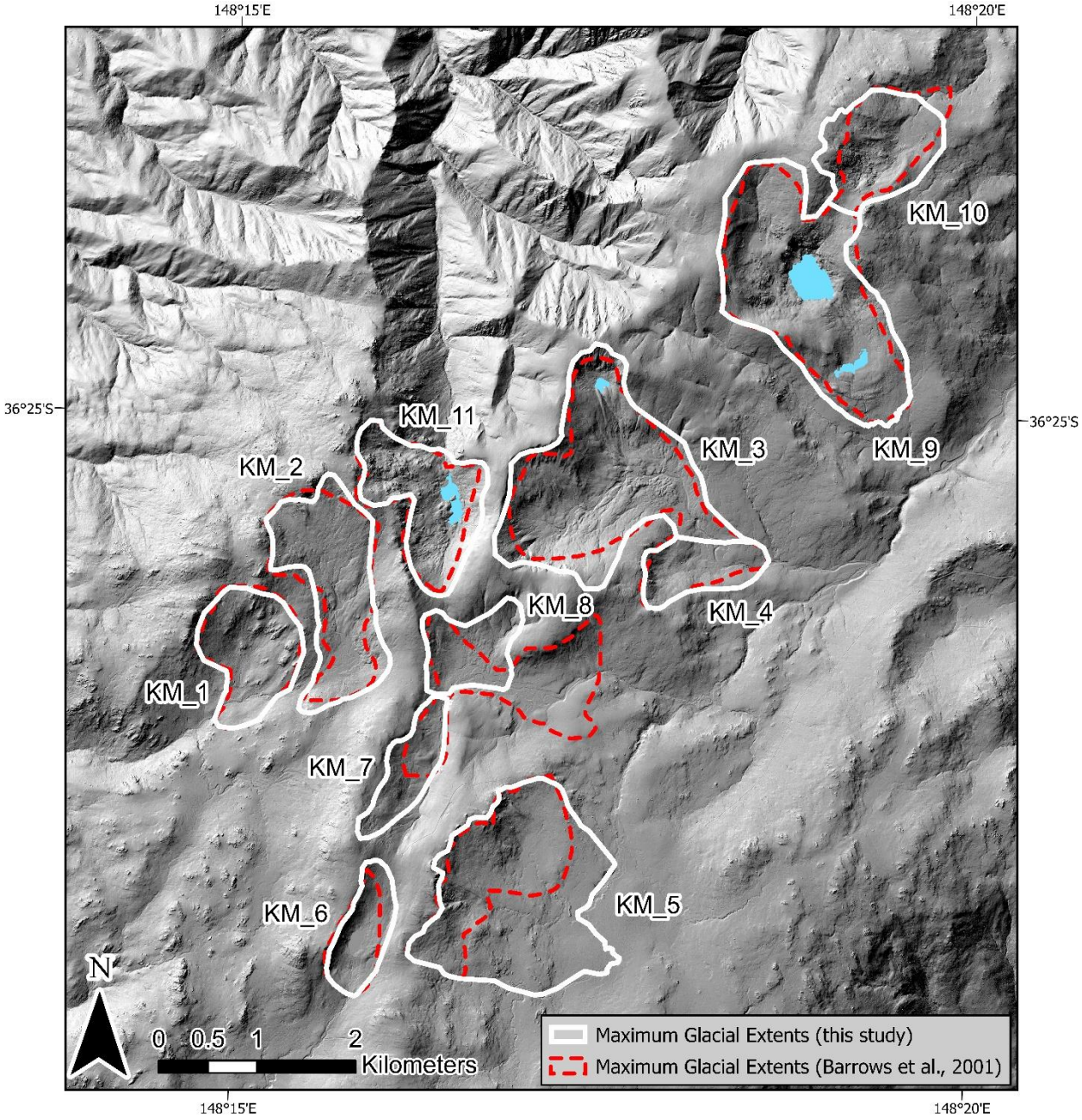

Figure 7. Comparison of maximum LGM glacial extents in the Snowy Mountains mapped by Barrows *et al*. (2001(red dashed lines) and maximum LGM glacial extents mapped in this study (white solid lines) based on lidar data. Lidar data from Gallant *et al*. (2011).

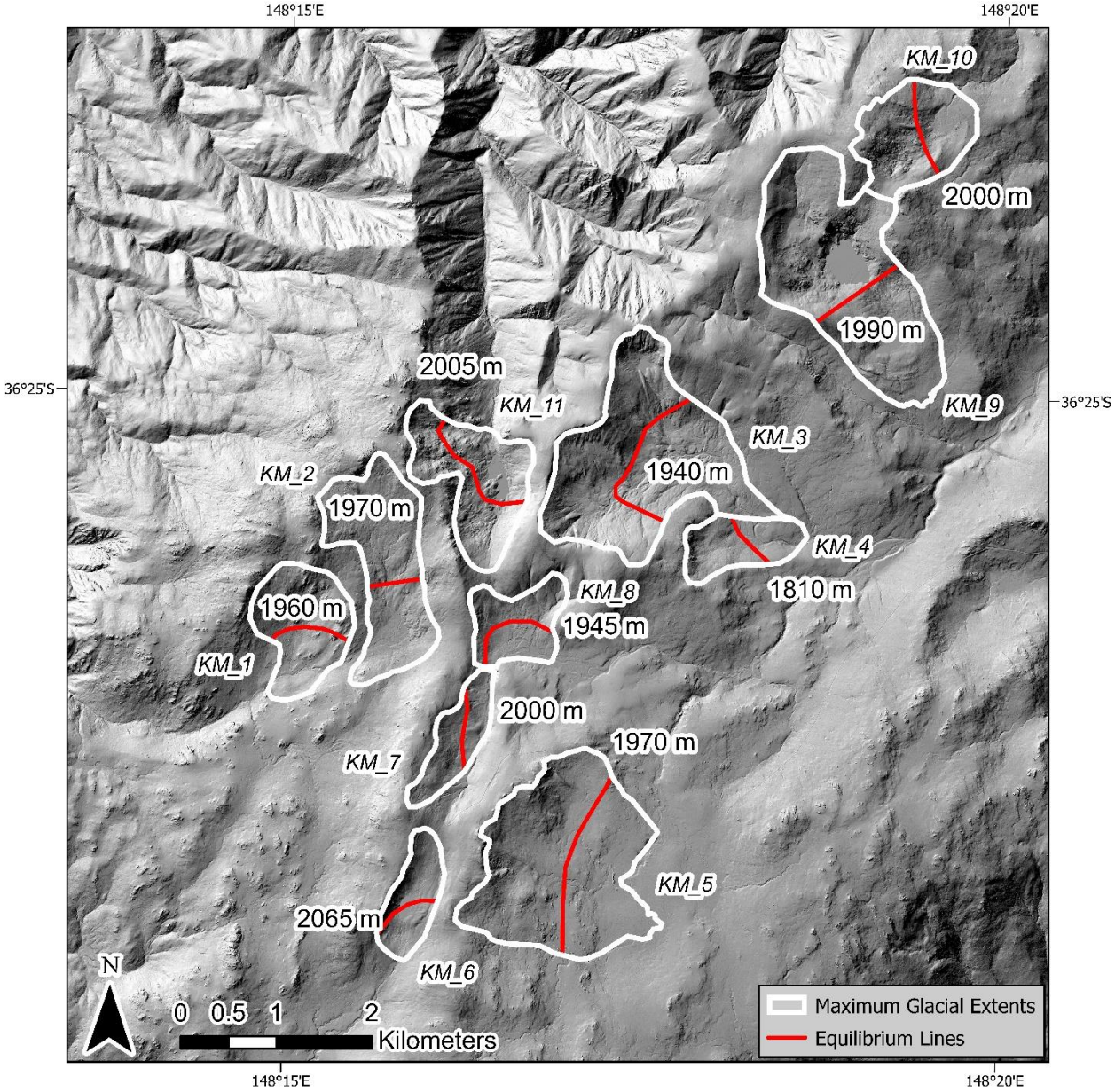

Figure 8. Equilibrium line altitudes (red) in the Snowy Mountains at maximum glacial extents (white outlines) during the LGM as determined by the AAR method. Lidar data from Gallant *et al*. (2011).

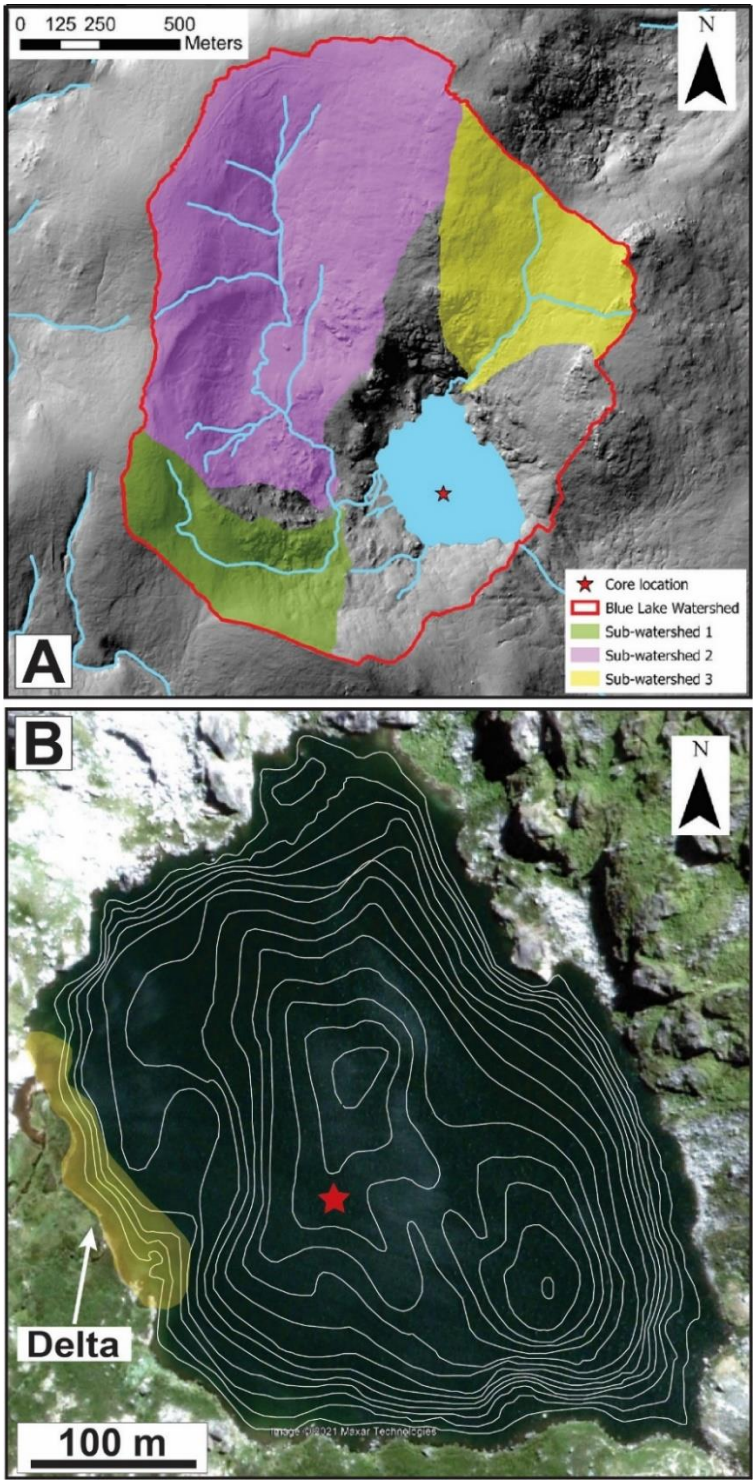

Figure 9. A) Sub-watersheds of largest streams within the Blue Lake catchment, and B) Satellite image of Blue Lake showing bathymetry (2-m contours; Dulhunty; 1945) and a small fan-delta on the western edge of the lake that is a plausible sediment source for turbidites found in units 1 and 11 (Figure 11). In both panels, the coring site is marked by the red star. Lidar data from Gallant *et al*. (2011), and satellite imagery (from February 2002) courtesy of Google Earth.

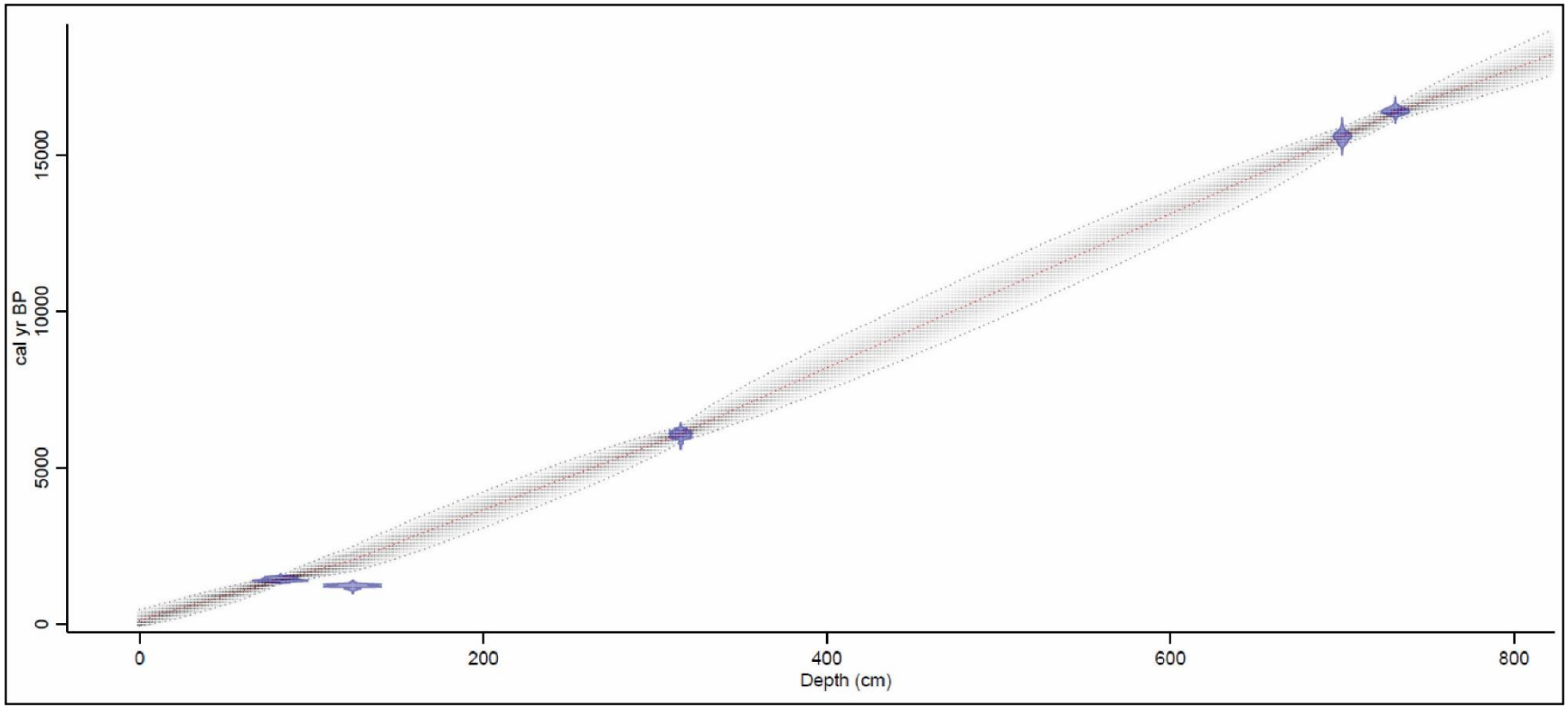

Figure 10. Age-depth model produced by Bacon (Blaauw and Christen, 2011) calibrated with SHCal20 (Hogg *et al.*, 2021) for core ABL16-LI. The blue regions show ^{14}C sample locations and uncertainties, the dotted red line indicates the mean model age trend, and the shaded gray region indicates the 2σ age windows.

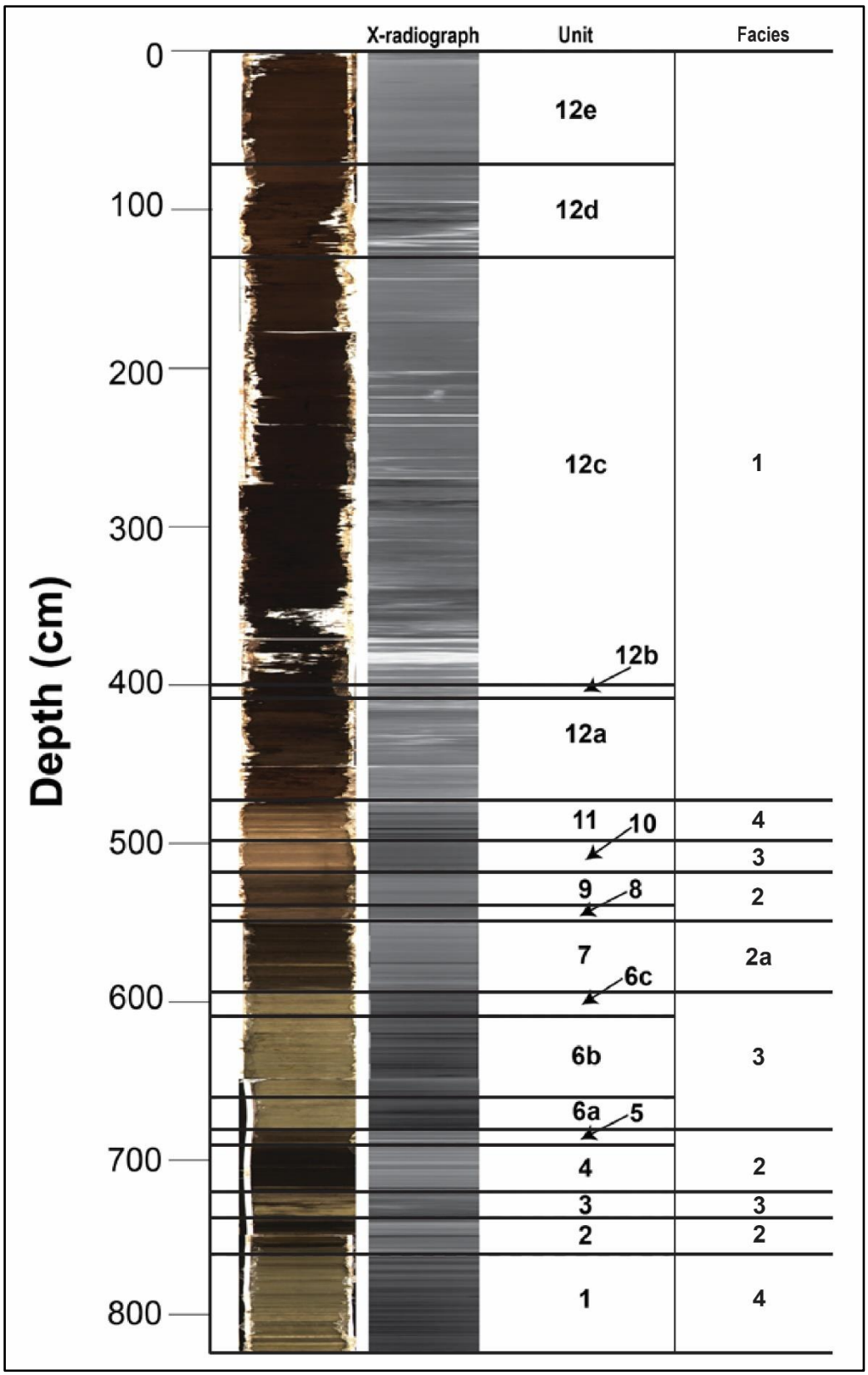

Figure 11. From left to right: Composite image scan of core ABL16-LI, composite X-radiographic scan, unit designations, and facies designations.

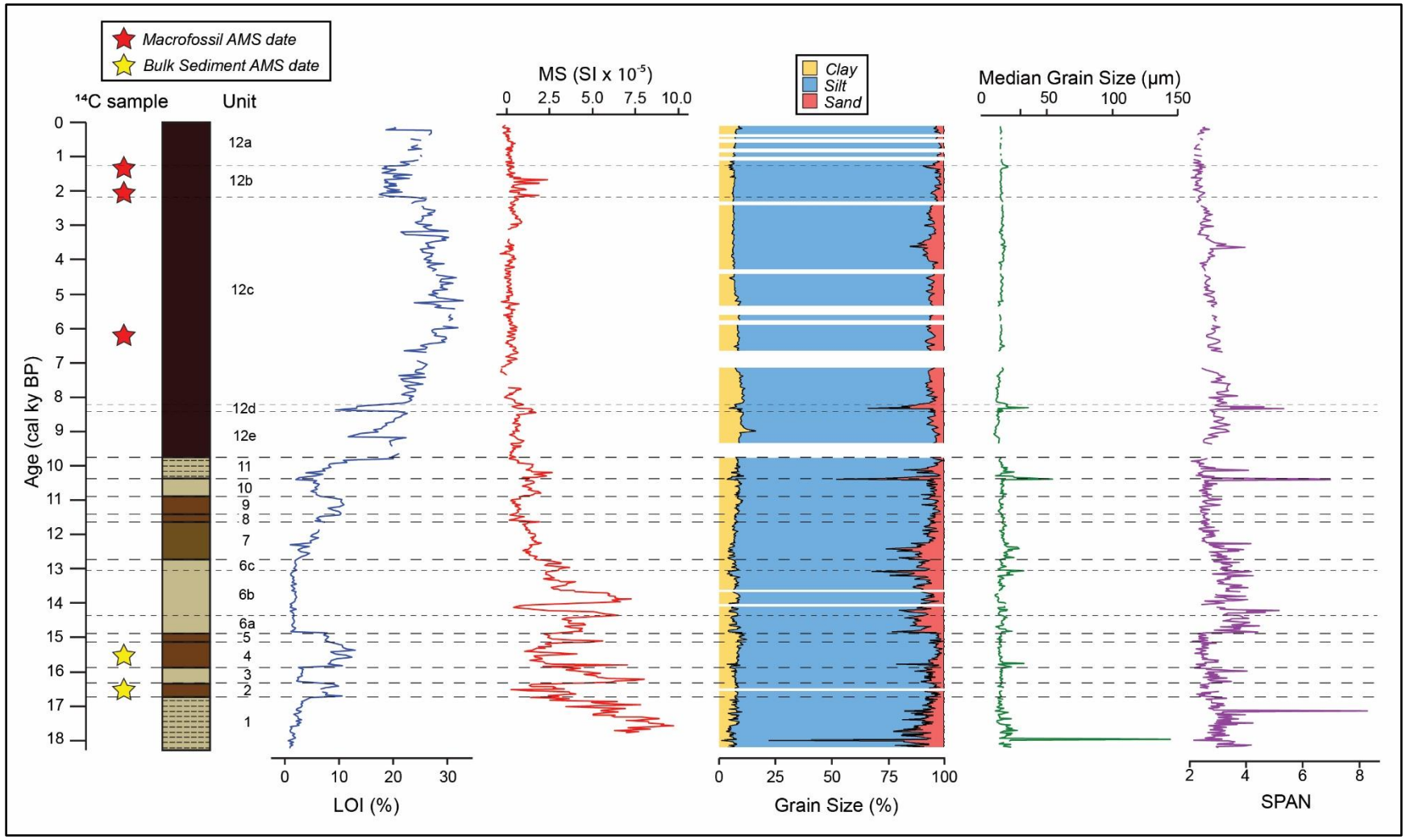

Figure 12. Composite data from core ABL16-LI relative to calibrated age model. Left-to-right: radiocarbon sample locations, simplified core facies, unit designations (Figure 11), loss-on-ignition (LOI), magnetic susceptibility (MS), grain size distribution in percent volume, median grain size, and SPAN (a dimensionless parameter assessing grain size variability within a sample). Gaps in data reflect intervals in the core where there was not enough sediment to sample.

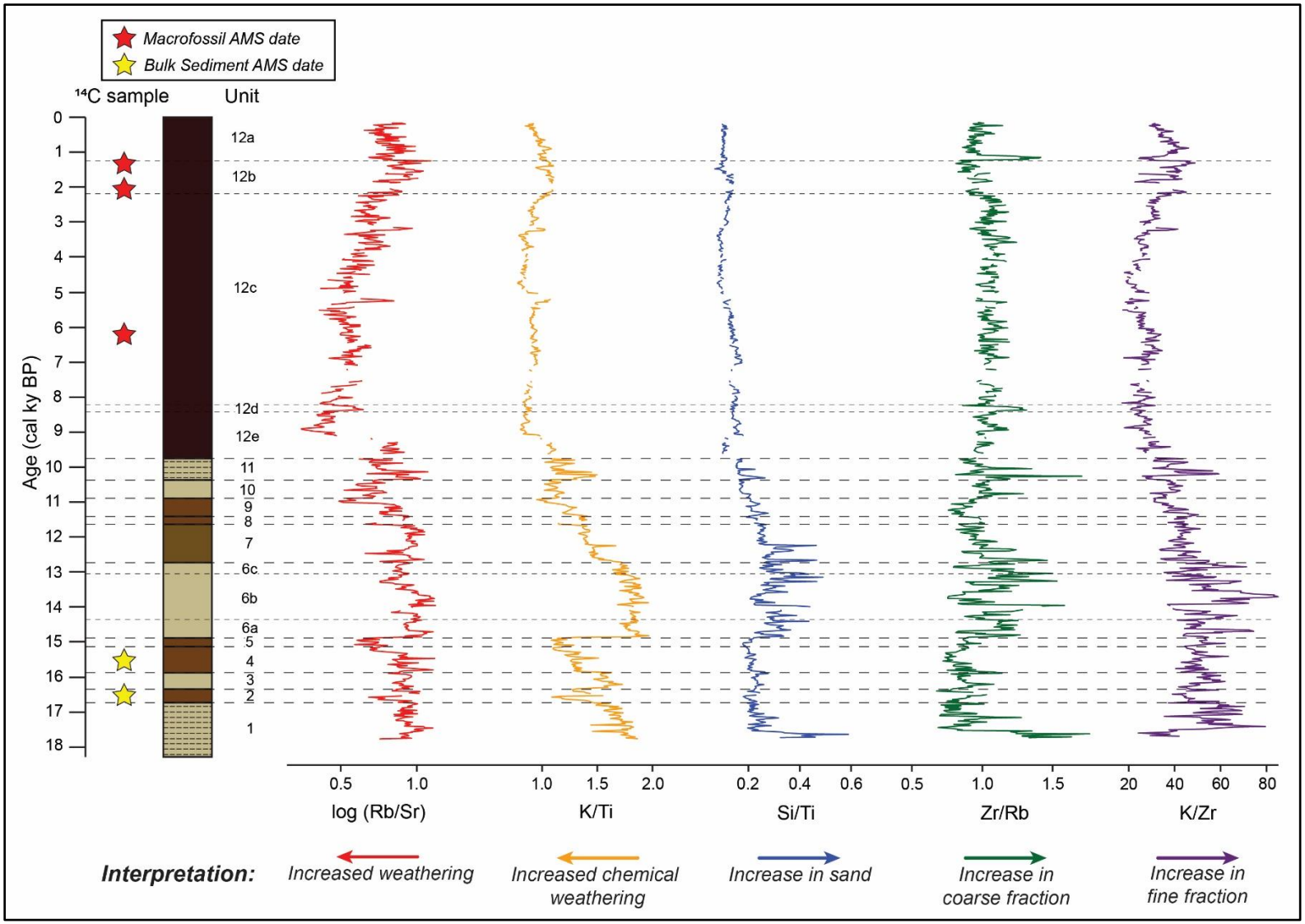

Figure 13. Composite data from core ABL16-LI relative to calibrated age model. Left-to-right: locations of radiocarbon samples, simplified core facies, unit designations, and XRF proxies including log(Rb/Sr), K/Ti, Si/Ti, Zr/Rb, and K/Zr, with their interpretations shown at the bottom. Gaps in data reflect intervals in the core where there was not enough sediment to sample.

Appendix A: Age-depth model for Blue Lake

I ran the Bacon age-depth model for core ABL16-LI with a variety of parameters and samples to generate the age-depth model used in this report. Several bulk sediment samples were ultimately excluded from the age-depth model because the Bacon program did not account for them or because I deemed them to be anomalous because they would require improbable shifts in sedimentation rates. Bulk sediment samples are inherently less reliable than terrestrial macrofossil samples because they can contain carbon from several sources. This introduces considerable uncertainty into the samples that cannot be easily accounted for – in essence, it is difficult to determine exactly what is being dated. A summary of the samples that were excluded from the final age-depth model is provided in Table 4.

Table 4. Depth in core and radiocarbon age of samples excluded from final age-depth model. 2σ calibrated ages were calibrated with the dataset from Reimer *et al*. (2020).

Sample ID	Lab ID	Depth (cm)	Material	^{14}C age (yr BP)	± yr (1σ)	Calibrated age ranges (2σ, yr BP)			
						Min	Max	Prob.	Median Prob.
ABL16-LI-82-s	187489	82	Bulk sed.	2000	25	1836 1867	1854 2001	0.035 0.965	1941
ABL16-LI-124-s	187490	124	Bulk sed.	2115	25	1934 1996	1952 2106	0.040 0.960	2042
ABL16-LI-315-s	187491	315	Bulk sed.	5600	35	6301	6446	1.000	6365
ABL16-LI-476-s	187492	476	Bulk sed.	5870	30	6502 6537	6516 6742	0.020 0.980	6647
ABL16-LI-591-s	187571	591	Bulk sed.	13350	70	15774	16241	1.000	16088

Samples ABL16-LI-82-s and ABL16-LI-315-s were used to calculate a reservoir effect but excluded from the age-depth model because more reliable plant macrofossil samples were available at the same depths. Sample ABL16-LI-124-s was also excluded from the age-depth model because of a paired plant macrofossil sample. Because of concerns surrounding the reliability of the paired plant macrofossil sample (ABL16-LI-124-m) discussed in section 5.2, I omitted this sample from the reservoir effect calculation. Samples ABL16-LI-476-s and ABL16-LI-591-s were omitted from the final age-depth model because they would result in unreasonable

sedimentation rate shifts that do not appear to be reflected in core stratigraphy or proxy data. Moreover, Bacon simulations do not appear to account for these samples when they are included in the age-depth model apart from very minor shifts in sedimentation rates (Figure 14). Instead, in the bottom half of the core the age-depth model is influenced by samples ABL16-LI-315-s, ABL16-LI-700-s, and ABL16-LI-731-s, and there is not a meaningful difference between including and excluding these samples. However, because these samples would require such an exceptional shift in sedimentation rates, I ultimately opted to exclude them and simplify the age-depth model.

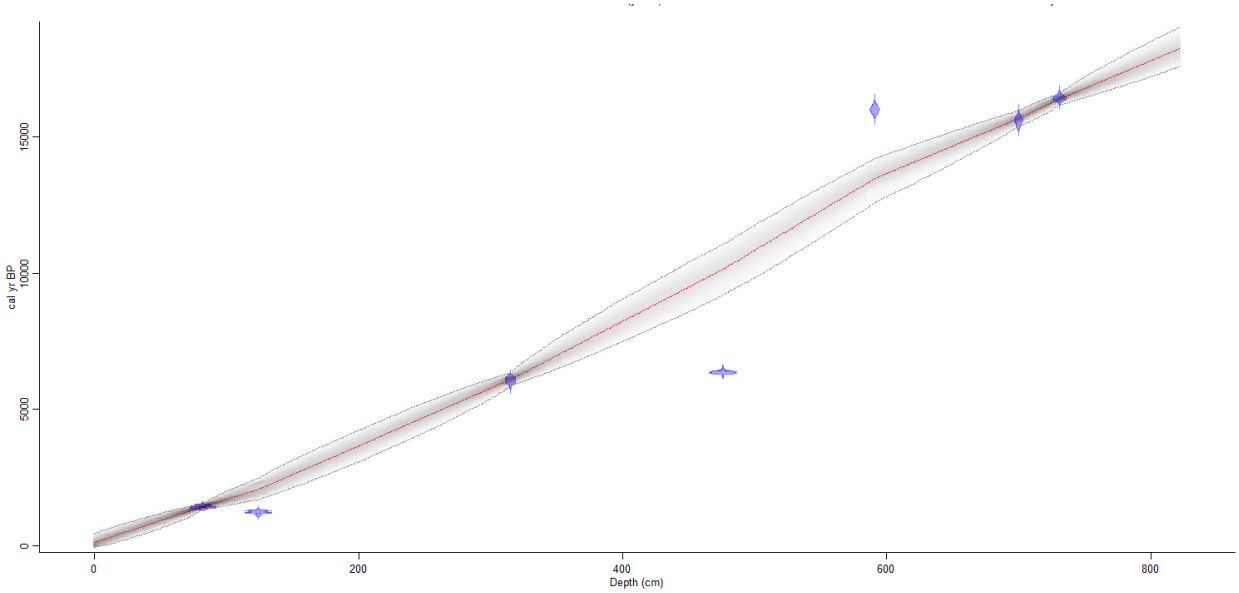

Figure 14. Age-depth model including samples ABL16-LI-476-s and ABL16-LI-591-s. These samples have a minimal effect on the overall age-depth model but suggest unreasonable sedimentation rates and were therefore omitted from the final model.